Climate Impacts of the El Niño-Southern Oscillation in Africa

Wenju Cai[1,2,3,*], Chris Reason[4], Elsa Mohino[5], Belen Rodríguez de Fonseca[5,6], Johan Malherbe[7], Agus Santoso[8,9,*], Xichen Li[10], Hector Chikoore[11], Hyacinth Nnamchi[12,13], Michael J. McPhaden[14], Noel Keenlyside[15,16,17], Andrea S. Taschetto[9], Lixin Wu[1,3], Benjamin Ng[2], Yi Liu[1], Tao Geng[3], Kai Yang[2], Guojian Wang[18], Fan Jia[19,3], Xiaopei Lin[1,3], Shujun Li[1,3], Yun Yang[20], Junkai Wang[1], Li Zhang[1,3], Ziguang Li[1], Pokam Wilfried[21], Liming Zhou[22], Xuebin Zhang[18], Francois Engelbrecht[23,24], Zhuoran Li[25], and Joseph N. Mutemi[26]

1. Physical Oceanography Laboratory/Frontiers Science Center for Deep Ocean Multispheres and Earth System/Sanya Oceanographic Institution, Ocean University of China, Qingdao, China
2. State Key Laboratory of Marine Environmental Science & College of Ocean and Earth Sciences, Xiamen University, Xiamen, China
3. Laoshan Laboratory, Qingdao, China
4. Department of Oceanography, University of Cape Town, Rondebosch, South Africa
5. Departamento de Física de la Tierra y Astrofísica, Facultad de Físicas, Universidad Complutense de Madrid, 28040 Madrid, Spain
6. Instituto de Geociencias, IGEO (UCM-CSIC), Madrid, Spain
7. Agricultural Research Council, Natural Resources and Engineering, Pretoria, South Africa
8. CLIVAR International Project Office, Qingdao, China
9. Climate Change Research Centre (CCRC), and ARC Centre of Excellence for Climate Extremes, University of New South Wales, Sydney, NSW, Australia
10. Institute of Atmospheric Physics, Chinese Academy of Sciences, Beijing, China
11. Department of Geography and Environmental Studies, University of Limpopo, Turfloop Campus, Sovenga 0727, South Africa
12. GEOMAR Helmholtz-Zentrum für Ozeanforschung Kiel, Kiel, Germany
13. Department of Geography, University of Nigeria, Nsukka, Nigeria
14. NOAA/Pacific Marine Environment Laboratory, Seattle, WA, USA
15. Geophysical Institute, University of Bergen, Bergen, Norway
16. Bjerknes Centre for Climate Research, University of Bergen, Bergen, Norway
17. Nansen Environmental and Remote Sensing Centre, Bergen, Norway
18. CSIRO Environment, Hobart, Australia
19. Key Laboratory of Ocean Observation and Forecasting and Key Laboratory of Ocean Circulation and Waves, Institute of Oceanology, Chinese Academy of Sciences, Qingdao, China
20. College of Global Change and Earth System Science, Beijing Normal University, Beijing, China
21. Department of Physics, Higher Teacher Training College, University of Yaounde 1, PO Box 47 Yaounde Cameroon
22. Department of Atmospheric and Environmental Sciences, University at Albany, State University of New York (SUNY), Albany, NY, 12222, USA
23. Climate Studies, Modelling and Environmental Health, CSIR Natural Resources and Environment, Pretoria, South Africa
24. GAES, University of the Witwatersrand, Pretoria, South Africa
25. Department of Environmental Studies, New York University, USA
26. Department of Earth & Climate Science, University of Nairobi, Kenya

*Correspondence to: Wenju Cai cwjresearch@gmail.com; Agus Santoso Agus.Santoso@clivar.org

Abstract

El Niño–Southern Oscillation (ENSO), alternating between warm El Niño and cold La Niña phases, profoundly affects climate of Africa, a continent strongly relying on rainfall for food security but has limited capacity to respond to natural hazards. For example, El Niño leads to drought over the Sahel and southern Africa but floods in east Africa, causing substantial impacts. This review synthesizes the understanding of ENSO impacts across Africa, elucidates

associated physical processes, and assesses the implications for modelling and projection of the impacts. ENSO forces anomalies in the tropical troposphere that are transmitted to Africa through planetary waves, drives tropical sea surface temperature variability in the neighbouring oceans, induces extratropical oceanic and atmospheric anomalies, and modifies regional circulations, whereby exerting an impact. The impact is different by ENSO events, asymmetric in amplitude and spatial pattern about El Niño and La Niña, and modulated by multidecadal variability. Under greenhouse warming, ENSO-induced dry and wet extremes are likely to increase over much of the continent. Therefore, it is vital to reduce uncertainty in ENSO impact in contemporary and future climates. Achieving this goal depends critically on a deeper understanding underpinned by global climate observations and improvements in climate modelling.

1. Introduction

The African continent, extending from the Mediterranean Sea at 37°N to the Cape Agulhas at 35°S in South Africa, is markedly distinguished by rainfall. Such distinction ranges from arid climate in the tropical Sahara, semiarid in the Sahel, countries of the Greater Horn of Africa and parts of southern Africa, to climate featuring scanty rain in southwestern southern Africa, and to summer monsoonal climate in west Africa, parts of eastern Africa and northern Madagascar island. Moisture is brought to the continent by winds from the Mediterranean Sea, the Atlantic, and the Indian Ocean[1-8] (**Box 1**). Hundreds of millions of people depend on seasonal rainfall to grow crop for foods.

El Niño-Southern Oscillation (ENSO), the most influential mode of climate variability originating in the Pacific, is a key factor modulating African rainfall. The ENSO impact on Africa has a strong seasonality concurrent with the main rainfall season; for example, the Sahel during boreal summer, East African rainfall during the short and long rain seasons, and southern Africa during austral summer[9,10,11,12,13] (**Box 1**). Complexity in how ENSO affects regional African rainfall involves modes of variability in the Indian and Atlantic Oceans[1,6], inter-basin interactions[14,15,16], and local circulation features[17,18,19,20,21,22,23,24,25,26,27,28,29], such as Somali Jet[16,17], tropical heat lows[18,19], South Indian Convergence Zone[21,22,23], and cloud band events[26,27,28] (**Box 1**).

The impact of ENSO is potentially devastating[30] as seen in a poignant example[31] during the drought in parts of southern Ethiopia, southern Somalia, and eastern Kenya from 2020 to 2023. Tens of millions suffered from acute food shortages, in part because of the 2020-2022 three-consecutive years of La Niña, which resulted in failed back-to-back rain seasons producing the most severe dry spell in decades. The crisis hit a region already grappling with poverty, leading to dire consequences: nearly one million children in Kenya suffered from acute malnutrition in 2022, while 3.3 million people across Kenya, Somalia, and Ethiopia were displaced from their homes[31]. Earlier, the 2016/17 La Niña compounded by the aftermath of the strong 2015/2016 El Niño led to an estimated 5-6 million people[32] facing food shortages in the same area. In southern Africa, the 2015/16 strong El Niño produced the most severe drought in

nearly 120 years, inflicting intense suffering on tens of millions[19]. Given the high vulnerability of the African society, it is paramount to enhance our understanding of the mechanisms dictating ENSO impact and the potential change in a warming climate.

In this review, we assess the current knowledge of ENSO impacts. We begin by describing mechanisms by which ENSO affects the climate through the Indian Ocean and the Atlantic Ocean, and modulation by the extratropical processes and regional circulations. We subsequently outline ENSO impact, its asymmetry between El Niño and La Niña and between strong and weak events, and multi-decadal fluctuations of the impact. We then discuss challenges in modelling ENSO impacts and in projecting their changes under greenhouse warming. The review ends on identifying pathways for progress.

2. Dynamical connections of ENSO to Africa

ENSO exerts its impacts on African climate through atmospheric teleconnections by tropical planetary wave propagation, and by sea surface temperature (SST) variability in the neighbouring oceans, whereby influencing the circulation over the continent. This section describes the main mechanisms by which ENSO impacts the African climate: through the troposphere, the Indian Ocean, and the Atlantic Ocean, and modulation extratropical processes and regional circulations. We focus on the dynamics associated with a typical El Niño or La Niña event.

The tropical tropospheric temperature

A fast pathway for impact is through the tropical troposphere. As El Niño develops in July August September (JAS), SST warm anomalies in the central and eastern equatorial Pacific cause an anomalous deep convection with anomalous ascending motion in the central and eastern equatorial Pacific but an anomalous subsidence over the western Pacific, weakening the Walker Circulation[10]. The anomalous deep convection drives a Gill-Matsuno response and the associated atmospheric Kelvin waves distribute the tropospheric heating over the eastern Pacific throughout the tropics (**Fig. 1a**), a process referred to as the tropospheric temperature mechanism[8,11,13]. The warm anomalies increase the atmospheric stability outside the Pacific, supressing atmospheric convection over West Africa[8] that leads to decreased rainfall in the Sahel[8,33]. In addition, the westward propagating Rossby waves drive high pressure anomalies over the tropical Atlantic, and the associated easterly wind anomalies over the Sahel weaken moisture transport from the Atlantic Ocean, decreasing Sahel rainfall[4]. The Rossby waves also weaken the Tropical Eastern African Jet, reducing the upper-level divergence over regions of the Horn of Africa[34,35].

The Indian Ocean

Tropical Indian Ocean SSTs are important agents for delivery of ENSO impacts. In JAS, the El Niño-induced western Pacific-minus-Indian Ocean zonal SST gradient weakens, intensifying convection over the Indian Ocean[36,37,38]. Upper-level anomalous westerlies via the Atlantic from enhanced convection in the central and eastern Pacific, together with anomalous easterlies from enhanced convection in the central

western Indian Ocean, form upper-level convergence, conducive to large-scale subsidence over the western Africa[4,36,37]. The anomalous circulations reinforce the effect from the troposphere warming mechanism, both unfavourable for rain over the Sahel.

During SON, El Niño exerts its impact often with a matured positive Indian Ocean Dipole (pIOD) (**Fig. 1b**), which develops through Bjerknes positive feedback similar to that operates in the Pacific. The weakened Walker circulation during El Niño induces equatorial easterly anomalies over the Indian Ocean, which often drive a concurrent pIOD event[38-41]. Cool anomalies near Sumatra-Java and warm SST anomalies in the western Indian Ocean cause a north-westward shift of atmospheric convection and a westward extension of the seasonal southeasterly trades[38,39,40]. The ITCZ becomes anomalously strong over the western Indian Ocean[39]. Thus, part of the ENSO impact in SON is conveyed via the IOD, which by itself exerts a similar impact to that of ENSO (comparing middle subpanel with ENSO and right subpanel without ENSO, Supplementary Fig. 1a).

In DJF, El Niño delivers its impact through warm anomalies of the Indian Ocean Basin mode (IOB) (**Fig. 1c**). El Niño-induced equatorial Indian Ocean easterly anomalies reduce the prevailing equatorial westerlies over the Indian Ocean[42]. The associated decrease in evaporative heat loss, together with the influence from tropospheric temperature warming, generates basin-wide warm anomalies[42], strengthening convection over the tropical Indian Ocean and weakening the pressure gradient between the ocean and the African continent[1,2,19]. The anomalous decrease in seasonal converging flows (from seasonal mean indicated by "light" arrows to anomalously weak indicated by "heavy" arrows, **Fig. 1c**) induces anomalies over much of southern Africa, including weaker southward excursion of the SICZ[20,7] (dashed blue lines, **Fig. 1c**), an intensified mid-level Botswana High[29], a weakened Angola Low and cloud bands[43] and a shallowed Mozambique Channel Trough[44].

El Niño-induced equatorward weakening of the subtropical highs drives a coherent negative phase of the Subtropical Indian Ocean Dipole and a coherent negative phase of the South Atlantic Subtropical Dipole[45,46,47], helping deliver El Niño impact to southern Africa. For example, the associated cold SST anomalies south of Madagascar decrease moist air from the subtropical South Indian Ocean towards southeastern Africa, favouring anomalously dry and hot summers over southern east Africa; to the north, the warm SST anomalies cause anomalously wet and cold conditions over east Africa[45] (Supplementary Fig. 1b). The impact becomes not statistically significant after ENSO influence is removed (comparing central and right subpanels of Supplementary Fig. 1b), suggesting that the Subtropical Indian Ocean Dipole is by and large a response to ENSO, facilitating ENSO impacts.

In MAM, the impact from El Niño through the ENSO-induced IOB wide warming continues unfavourable to southward transport of moisture into southern Africa. The IOB warming increases the Indian-minus-Pacific basin-scale SST gradient, conducive to easterlies over the western Pacific.. Some El Niño events transition into a

developing La Niña. As the transition occurs, convection over the western equatorial Pacific intensifies, creating an anomalously strong Walker circulation over the Indian Ocean[32,48] which strengthens the upper-level easterlies, increasing subsidence over eastern Africa.

The Atlantic Ocean

Atlantic Niño, or its opposite pahse, Atlantic Niña, operates in a positive feedback process reminiscent of and often concurrent with a La Niña, or El Niño, respectively. During an Atlantic Niña, anomalous easterlies drive increased upwelling, leading to cooling in the east, which, in turn, intensifies the anomalous easterlies[12,13,14,49]. The cold anomalies in the equatorial eastern Atlantic suppress atmospheric convection over the ocean and shift the tropical rain belt and the ITCZ northward. The equatorial Atlantic cold SST anomalies intensify the land–ocean thermal gradient and the land-ocean pressure gradient, strengthening the northward monsoon penetration into West Africa[5]. The associated anomalies feature a rainfall-dipole anomaly pattern with decreased rainfall over the Guinea coast but a tendency of increased rainfall in the Sahel[6,7] (Supplementary Fig. 1c).

When La Niña/El Niño occurs concurrently with Atlantic Niño/Niña, the latter helps deliver or reinforce ENSO impacts. For example, an Atlantic Niña often occurs in conjunction with an El Niño (**Fig. 1d**), reinforcing El Niño-induced dry anomalies to the Guinea coast but tending to induce wet anomalies over the Sahel[6,7]. The wet anomalies could be offset by the increased subsidence arising from the tropospheric temperature mechanism[11,12,13,14] (grey allows, **Fig. 1d**), rendering the rainfall-dipole anomaly pattern unstable. When an Atlantic Niña and an increase in subsidence over the Sahel are both dominated by an El Niño, spatially coherent dry conditions occur from Senegal to Ethiopia accompanied by anomalously high air temperatures in sub-Saharan Africa[50]. Thus, the concurrent Atlantic Niña helps broaden the El Niño-induced drying.

Modulations of ENSO impact on Africa

In addition to the influence conducted via tropical SST, ENSO's impact on African climate is modulated by extratropical oceanic anomalies such as Mediterranean SSTs, mid-to-high latitude variability such as the southern annular mode (SAM), and regional circulations including the Sahara Heat Low, the Angola Low, the Boswana High, and the SICZ. These circulation systems may respond to ENSO, but also vary independently, modulating ENSO impact. In this section, we discuss these processes.

Mediterranean SSTs. Warmer than normal Mediterranean SSTs enhances local evaporation, leading to advection of more moisture through the climatological winds, which increases continental moisture flux convergence in low-level northern Africa[51]. The consequence includes a northward migration of the rainband and an intensified monsoon[51,52], an impact comparable in amplitude to that from ENSO, substantially modifying ENSO impacts[51]. Further, the anomalously high SSTs in the eastern Mediterranean relative to the Indian Ocean strengthen low-level convergence between

the northeasterly moisture transport from the eastern Mediterranean and the monsoonal southwesterly moisture transport from the eastern equatorial Atlantic, conducive to increased rainfall over the Sudan-Sahel region[52]. Thus, the Mediterranean SSTs can substantially modify ENSO impact.

The SAM. A negative phase of the SAM reflects an equatorward shift of midlatitude westerlies. The associated frontal systems[53], and low-level moisture fluxes toward southern Africa, favourable for the mid-level uplift and low-level convergence, increasing winter rainfall in western South Africa[54]. However, in DJF, the associated easterly flows from the Indian Ocean to eastern South Africa decrease[55], reducing rainfall over the east. An equatorward shift of the atmosphere circulation during El Niño tends to induce a negative phase of the SAM, reinforcing El Niño-induced dry conditions over South Africa.

Regional circulations. Regional circulation systems over and surrounding Africa undergo considerable variations independent of ENSO, but also respond to ENSO. Variability of these regional systems, each alone or several combined, contributes to inter-event variations in ENSO impact.

Situated over the Saharan region in the summer months, the Saharan Heat Low fluctuates in intensity on time scales from intraseasonal, interannual, to interdecadal or longer[56,57]. The low pressure, combined with the relatively high pressure over the Guinean coast, produces a low-level pressure gradient, which is a driver of the West African monsoon such that the stronger the heat low, the more intense the monsoonal flow[56]. An intensified Saharan Heat Low favours African Easterly Jet at mid-level atmosphere[58] and occurrences of convection over the Central and Eastern Sahel, but a decrease in the convective activity and rainfall from Senegal to the West of the Jos Plateau[57]. Thus, variability of the heat low modifies ENSO impact.

Developing during April, May, and June, the Somali jet transits Kenya, Somalia and the Sahel, along the way bringing moisture and rainfall northward to the southern slopes of the Ethiopian plateau and the Greater Horn of Africa[17,59]. As such, a stronger jet is associated with anomalously high rainfall, whereas a weaker jet is associated with an anomalously dry condition over southern Ethiopia[60,61]. During El Niño, the Somali Jet onset tends to be later and the intensity is weaker such that many drought years over the Ethiopian plateau coincide with an El Niño[16,61].

The Congo Air Boundary breaks down in austral summer and is replaced by convectively active and moist convergence zone, facilitating tropical lows[18,62]. Like weak tropical cyclones, tropical lows occur in summer over tropical southern Africa and aggregate in the seasonal mean to form the Angola Low, contributing to rainfall variability in the tropical edge[18]. An anomalously weak and northward Angola Low promotes increased rainfall over tropical southern Africa but decreased rainfall over

subtropical southern Africa[62]; the reverse prevails for an anomalously southward Angola Low. The Angola Low shifts northward during El Niño but southward during La Niña[18]. Variability of the Angola Low modulates ENSO impact on Africa[63]; for example, during the 1997/98 event, the Angola Low hardly weakened, and an expected drought did not occur in southern Africa[19].

Tropical Temperate Trough links the tropics and the extra-tropics across southern Africa[28,43,64,65], and is a cloud band system of convergence and convection extending along the northwest-southeast direction over landmass to the southwest Indian Ocean, inducing heavy rainfall over southern Africa. During El Niño, the convergence is anomalously northwards, the troughs tend to be less common, as tropical lows are weaker and further north[18,62]; during La Niña phase, the trough forms more frequently and further south[18,43,62,66]. However, like the Angola Low, the trough varies independently of ENSO, modulating ENSO's impact. For example, during the 1997/98 El Niño event, a quick succession of two trough events, a 7-day wet spell during 1–7 January 1998, contributed to more than 40% of the 1997/1998 summer rainfall over much of South Africa[67].

The SICZ is a large-scale summer land-based convergence zone, extending across southern Africa into the southwest Indian Ocean, with position and intensity partially determined by surface conditions over southern Africa, particularly, zonal winds[20,68]. During El Niño, the SICZ shifts northeastward because of a weakening in the western portion of the South Indian High[20], reducing moisture transport from the Indian Ocean[69], contributing to a dipole pattern of rainfall anomalies, wet to the northeast and dry to the southwest.

Situated to the south and southeast of the heavy precipitation region across tropical southern Africa, the Boswana High typically forms in August, strengthens and moves southward over southern Africa during austral spring and summer[29,70,71]. The strength of the high varies independently of ENSO; for example, large anomalies in the Botswana High are observed in a number of neutral ENSO summers when Southern Africa is unusually wet or dry[70]. However, the high tends to intensify during El Niño summers and weakens during La Niña winters[70,71]. For example, during the 2015/16 El Niño event, an anomalously strong Botswana High and associated southwesterlies over Tanzania and northern Mozambique reduced moisture entering the continent from the tropical Indian Ocean; consequently, extremely dry conditions occurred across most of southern Africa[19]. Nevertheless, the magnitude of the Botswana High anomalies is not proportional to the strength of ENSO events. For example, the High during the 1997/98 strong El Niño event was less intense than the weaker 1986/1987 El Niño event[19,71], contributing to a condition against an expected severe dry season in 1997/98.

3. ENSO effects

So far, we have described the mechanisms whereby ENSO affects Africa climate, assuming that El Niño and La Niña are symmetric in amplitude and in anomaly pattern, and that the mechanisms are stable over time. In this section, we describe ENSO effect on African climate. We then turn to asymmetric impact between El Niño and La Niña, impacts of different ENSO flavours, and decadal and multidecadal fluctuations.

Symmetric depiction

During El Niño-developing JAS, Sahel is drier and hotter than normal (**Fig. 2a**) (Supplementary Fig. 2a). The increased atmospheric stability due to increased convection in the equatorial central and eastern Pacific supresses atmospheric convection over West Africa[8], and weakens the circulation and moisture transport, leading to decreased rainfall in the Sahel[8,33]. Further, as a result of convergence from the Atlantic and the Indian Ocean, upper-level anomalously increased subsidence over western Africa[4] decreases rainfall over the Guinea coast in late boreal spring and subsequently over the Sahel in the peak season of West African monsoon, with a commensurate reduction in the frequency of wet days and heavy rainfall events[4,36,37]. Occasionally, the ocean warm anomalies after an El Niño may persist into boreal summer; for example, remnant warm anomalies from the 1982/83 strong El Niño led to the 1983 boreal summer drought over the western Sahel[72], inducing one of the driest summers in the twentieth century record for the region. Conversely, during a La Niña-developing JAS, a tropospheric cooling promotes atmosphere instability over the Sahel. In addition, upper-level anomalous easterlies from enhanced convection in the western Pacific via the Atlantic together with anomalous westerlies from decreased convection in the central and western Indian Ocean, drives an upper-level divergence, conducive to a large-scale ascendence over the western Africa[4]. Typically, ENSO-induced Sahel JAS rainfall anomaly over the Sahel (17°W-40°E,11°N-15°N) is 0.42 mm day^{-1} °C^{-1} of Niño3.4 SST.

As El Niño develops, eastern and central Africa short rain increases (**Fig. 2b**) although surface temperature anomalies are less clear because the associated increase in evaporative cooling offset the warm anomalies (Supplementary Fig. 2b). The weakened Walker circulation, the anomalous equatorial easterlies associated with a concurrent pIOD event, and the anomalously strong ITCZ over the western Indian Ocean[39] promote low-level warm moist convergence toward the equatorial east coast of Africa. As a result, anomalously high rainfall occurs during the short-rain season over the eastern and central Africa countries[38,39,40,41]. For example, during the 1997 El Niño event, devastating floods in Somalia, Ethiopia, Kenya, Sudan and Uganda caused several thousand deaths and displaced hundreds of thousands of people[38]. During La Niña, anomalous westerlies over the equatorial Indian Ocean associated with the increased Walker circulation shift low-level convergence to the eastern Indian Ocean/western Pacific region, causing drier than normal conditions over eastern Africa. For example, the 2020-22 three-consecutive years of La Niña led to failed rain seasons with food shortage and acute malnutrition across Kenya, Somalia, and Ethiopia[31]. Typically, ENSO-induced rainfall anomaly during the short-rain season over eastern Africa region (29°E-42°E,7°S-5°N) is +0.38 mm day^{-1} °C^{-1} of Niño3.4 SST.

During El Niño, southern Africa (south of ~15ºS) experiences warmer and drier conditions in austral summer (**Fig. 2c**) (Supplementary Fig. 2c) as low-level moisture convergence and cloud band development are suppressed[43]. The suppression occurs as El Niño-induced strengthening in convection over the tropical Indian Ocean and El Niño-induced weakening in the pressure gradient between the ocean and the African continent increase subsidence over much of southern Africa. By contrast, over off-equatorial East Africa, above-average rainfall occurs because the seasonal southward excursion of the SICZ and cloud band events are impeded and shift northeastward to the off-equatorial regions[20,43]. These processes drive the north-wet and south-dry rainfall dipole (+0.29 and -0.26 mm day^{-1} ºC^{-1} of Niño3.4 SST, respectively) (**Fig. 2c**), accompanied by warm anomalies to the south (Supplementary Fig. 2c). In MAM, as the El Niño-induced IOB warming continues, the dry and warm condition persists in southern Africa (**Fig. 2d**) (Supplementary Fig. 2d). In addition, El Niño-induced negative phase of the Subtropical Indian Ocean Dipole, with its cold pole to the south[45,46,47], helps deliver El Niño impact to southern Africa, reinforcing the anomalously dry and hot conditions over southern east Africa and anomalously wet and cold conditions over east Africa[45]. During La Niña, the impact reverses. For example, a weakening in convection over the tropical Indian Ocean and an intensification in the pressure gradient between the ocean and the African continent increases low-level moisture convergence facilitating cloud band development over land[43], leading to colder and wetter conditions south of ~15ºS. Over off-equatorial East Africa, below-average rainfall occurs as the SICZ and cloud band events extend further south, leading to a rainfall dipole, accompanied by warm anomalies to the south, a pattern that persists to the MAM season.

Asymmetric impact

El Niño and La Niña events are not symmetric in amplitude or spatial pattern, rendering that their impacts on African climate are not either. For example, the SST anomaly centre, that is, position of maximum anomalies, can be in the equatorial eastern Pacific (EP-ENSO) or in the equatorial central Pacific (CP-ENSO)[73,74,75,76,77,78]. The amplitude of EP-El Niño is greater than that of CP El Niño[73,74,75,77,78], whereas the amplitude of CP La Niña tends to be greater than that of EP La Niña[73,74,,79,80,81]. Additionally, the amplitude of strong El Niño, which tends to be an EP El Niño[59,61,63], is greater than that of a strong CP La Niña. A La Niña event tends to last for multiple years but such a long duration is rarely seen for El Niño. As a result of the diversity, impacts of El Niño and La Niña are asymmetric. In this section, we outline the implications of ENSO asymmetry for ENSO impacts on Africa. We use a linear combination of the first two empirical orthogonal functions of DJF SST anomalies in the tropical Pacific to construct indices of EP and CP ENSO[74, 76,77,78]. Defining an event as when the corresponding index is greater than one standard deviation value in amplitude (Supplementary Fig. 3a, b), we construct composites of African rainfall anomalies during ENSO events.

Because of the ENSO diversity and asymmetry between El Niño and La Niña, rainfall anomalies of EP El Niño are stronger and more spatially coherent than rainfall anomalies of CP El Niño[82,83,84]; by contrast, rainfall anomalies of CP La Niña are stronger and better-defined than those of EP La Niña[82,83,84] (Supplementary Fig. 3).

These differences are in part due to a greater EP El Niño amplitude than that of CP El Niño and different locations of the anomaly centres[73,74,75,]. Overall, in most seasons, the opposite polarity between El Niño and La Niña years is due to the opposite anomalies of EP El Niño and CP La Niña (**Fig. 2e-2h and 2i-2l**) (Supplementary Fig. 2i-2l and 2e-2h). The same is true for air temperature anomalies; that is, anomaly during EP El Niño is greater than that during CP El Niño, but greater during CP La Niña than during EP La Niña (Supplementary Figs 2 and 4).

In the Sahel region, owing to the large amplitude of EP El Niño, and a strong cooling in the equatorial eastern Atlantic coherent with EP El Niño[85], dry anomaly in JAS averaged across EP El Niño events (**Fig. 2e**) is -0.73 mm day^{-1}, larger than -0.12 mm day^{-1} averaged across CP El Niño events when the anomaly is weak and elusive (Supplementary Fig. 3). Towards the Guinea coast, EP El Niño shows a drying in DJF (**Fig. 2g**), owing to an associated increase in subsidence over the equatorial eastern Atlantic arising from increased convection over the western Indian Ocean[12,73]; such dry anomalies are not seen during CP El Niño (Supplementary Fig. 3). By contrast, because CP La Niña is stronger than EP La Niña in amplitude, CP La Niña-induced wet anomaly in the Sahel in JAS (**Fig. 2i**) is +0.30 mm day^{-1}, greater than +0.12 mm day^{-1} during EP La Niña.

In the east Africa region, short-rain wet anomaly during EP El Niño (**Fig. 2f)** is greater than that during CP El Niño[83], +0.90 mm day^{-1} and +0.22 mm day^{-1}, respectively. Because of the greater CP La Niña amplitude than that of EP La Niña, CP La Niña-induced east Africa dry anomaly in the short-rain season is well-defined (**Fig. 2j**); averaged across events, the dry anomaly is -0.27 mm day^{-1}. By contrast, during EP La Niña, dry anomaly is hardly observed (second panel from left, Supplementary Fig. 3d). In amplitude, EP El Niño-induced wet anomaly is greater than CP La Niña-induced dry anomaly, +0.90 and -0.27 mm day^{-1}, respectively, in part because a pIOD induced by EP El Niño is greater than an nIOD induced by CP La Niña[78].

In the long-rain season, because a CP La Niña often persists into a multiyear La Niña event[79], the associated eastward shift of convergence toward the Indo-Pacific region induces a dry anomaly (-0.38 mm day^{-1}) over east Africa (**Fig. 2l**). There is no counterpart for EP El Niño as a strong El Niño event usually does not continue into the next year. Instead, El Niño events often transition into a developing La Niña[74,79]. The transition leads to a dry short-rain season in east Africa[1,32]. During such transition, when SST in the tropical western Pacific is high in MAM[32], drawing moisture to the west, rainfall decreases in the long-rain season, generating a rainfall decrease in both short and long rain seasons. Such a sequence occurred in 2016-2017, when the 2015/16 El Niño transitioned to a La Niña, leading to a lack of water for socio-economic activities with severe consequences such as food insecurity[30,31,32].

Over southern Africa, the EP El Niño-induced anomalous summer rainfall diploe, with a dry anomaly of -0.70 mm day^{-1} in the south and a wet anomaly of +0.72 mm day^{-1} in the equatorial eastern Africa (**Fig. 2g**). The dipole is generated owing to a decreased convergence over southern Africa, an anomalously weak poleward excursion of the converging flows from the Atlantic and the Indian Ocean, and a

northeastward shift of regional circulation features[20,43] such as the SICZ and cloud band events. During CP La Niña, a dipole of opposite polarity occurs, with a wet anomaly in the south of +0.64 mm day^{-1} and a dry anomaly of -0.33 mm day^{-1} in the north, respectively. During either CP El Niño or EP La Niña, the dipole is not as well-defined and anomalies are small[83] (Supplementary Fig. 3e).

Multidecadal variability

Adding to the complexity is that the ENSO impact and the African climate are not stable over time[6,36,87,88] but fluctuate on multidecadal time scales. The fluctuation of ENSO impact is a result of many factors, including varying ENSO amplitude, its co-variability with modes of interannual variability of the other oceans, and multidecadal rainfall variability driven by multidecadal SST fluctuations that might exacerbate ENSO impacts.

For example, ENSO impact on Sahel rainfall is strong during the 40 years of 1971-2010, when modes of variability of the three oceans were coherent than the 40 years before 1970 (ref.[6,7,36,87,88,89]). By contrast, before the 1970s, El Niño is weak[90,91], and an El Niño-induced decrease in West Africa rainfall was weak and sometimes did not occur (**Fig. 3a,** compare the spatial anomalies); in part because cold SSTs averaged across the tropical oceans, relative to SSTs in the North Atlantic, are inconducive for an El Niño to induce a dry condition over the Sahel[92]. Further, co-variability of an El Niño with an Atlantic Niña was low, and the Atlantic Niño-induced rainfall anomaly dipole was more conspicuous. During 1971-2010, a negative phase of Atlantic Multidecadal Variability enhanced co-variability between Pacific El Niño/La Niña and Atlantic Niña/Niño[6,15,93], decreasing occurrences of the rainfall dipole pattern associated with Atlantic Niño/Niña. For instance, the rainfall dipole pattern associated with an Atlantic Niño disappeared[6,36,94], as the anomaly of low Sahel rainfall from Atlantic Niño was overwhelmed by anomalously high rainfall associated with a Pacific La Niña[95,96]. The pan-West Africa influence by ENSO since the 1970s[36,89] is partly induced by enhanced co-variability between an El Niño and a developing positive IOD, which enhances western tropical Indian Ocean convection, leading to decreased rainfall over West Africa[97].

Similarly, substantial decadal fluctuations in ENSO impact occur in East Africa-ENSO teleconnections**.** For example, during the 1971-2010 period, an enhanced ENSO-IOD coupling[97] intensifies the associated East Africa short-rain response to ENSO[98] (**Fig. 3b**). An El Niño during the 1971-2010 period saw strong equatorial Indian Ocean easterlies and a westward shift in the Indian Ocean ITCZ, conducive to a strong wet anomaly over the Horn of Africa accompanied by a strong dry anomaly over the southern part of eastern Africa[48]. Since around the turn of the

21st century, a decreased ENSO-IOD relationship[99] contributes to the observed reduction in the impact of El Niño on east Africa rainfall.

Likewise, during the 1970-2010 period, ENSO impact on southern Africa summer rainfall intensified, characterized by the dipole pattern of rainfall anomalies featuring wet equatorial eastern but dry southern Africa during El Niño[100] (**Fig. 3c**). The strengthened ENSO-IOD coupling during 1971-2010 induced strong DJF warm anomalies in the equatorial and tropical southern Indian Ocean. The strong Pacific-Indian Ocean coupling led to a DJF reversal of the Walker circulation over the western tropical Indian Ocean[101] and a strong negative SIOD[102], both contributing to the low rainfall in southern Africa. Additionally, a positive phase of the Interdecadal Pacific Oscillation is associated with more El Niño events and an overall stronger impact by the ENSO on southern Africa[103].

Rainfall variability driven by multidecadal SST fluctuations exacerbates the impacts of ENSO. The strongest multidecadal rainfall variability is observed over the Sahel (**Fig. 3d**)**.** For example, the positive phase of the Interdecadal Pacific Oscillation (IPO), with warm anomalies in the tropical Pacific, from the late 1960s to the late 1980s contributed to a widespread decrease in Sahel JAS rainfall[95,104] (**Fig. 3e, red box**) such that El Niño remnant SST anomalies in 1983 over the Indian Ocean induced a near-record Sahel drought[72]. A positive phase of the IPO is associated with reduced moisture convergence and vertical ascent over the south African subcontinent, resulting in a substantial reduction in tropical–extratropical cloud band formation and rainfall[105] (**Fig. 3e, purple box**). Regions centered on the Limpopo River Basin experience distinctive rainfall variability on a 17-20-year timescale, with anomalously low rainfall when the equatorial Pacific SSTs display a patten reminiscent of a positive IPO[106]. Conversely, the negative phase of the IPO since the 1990s contributes to the Sahel rainfall recovery[95,104]. The cooling in the East Pacific relative to the West Pacific associated with the negative IPO induced a decrease in East Africa long rain[107,108] (**Fig. 3e, green box**) and generated a greater susceptibility to long-rain drought during La Niña events, heightening the risk of consecutive short and long rain droughts[32]. The strengthened Walker circulation post-1990s results in warming in the central and eastern Indian Ocean[109], reducing moisture transport to the equatorial Eastern Africa, leading to drying over the region[110].

A positive phase of the Atlantic Multidecadal Variability (AMV), with higher SSTs in the tropical North Atlantic and Mediterranean Sea, relative to the tropical South Atlantic, increases meridional moisture convergence over the Sahel region, and a northward migration of the ITCZ, cloud band events conducive to Sahel rainfall[33,95,111] (**Fig. 3f**). Through this mechanism, the negative AMV during the 1960-1980 period

decreased northern-minus-southern hemispheric gradient and contributed to the drying of the Sahel during the 1960-1980s, whereas the positive phase since 1980s promoted enhanced rainfall and dominated the recovery[95,112], with a commensurate change in the frequency of extreme rainfall, particularly during La Niña[113]. The post-1990 positive AMV phase, conductive to equatorial Pacific easterlies that reinforce the negative IPO[114,115,116], contributes to the Sahel rainfall recovery.

4. Modelling ENSO impacts

Modelling ENSO impacts on African climate is challenging, because not only ENSO SST anomalies within the Pacific but also SSTs outside the Pacific are essential. For example, for impact on the Sahel, higher JJA SSTs in the Indian Ocean relative to SSTs in the Mediterranean decrease moisture convergence and rainfall over the west Sahel[51,52]; El Niño-induced warm SST anomalies over the Indian Ocean prolonged the 1982 El Niño-induced Sahel drought[72]; and whether an El Niño leads to lower-than-normal rainfall over the Sahel depends on whether the tropical ocean as a whole is warmer than the subtropical North Atlantic[92]. For impact on east Africa, Indian Ocean SST anomalies associated with development of a pIOD deliver an El Niño-induced rainfall increase in the short rain season over eastern Africa[40]. For southern Africa, El Niño-induced IOB warm SST anomalies over the tropical Indian Ocean limit southward moisture transport and moisture convergence toward southern Africa, and curtail a southward excursion of the SICZ[20], the Angola Low, and Tropical Temperate Troughs[18,43]. Realistic modelling of SST variability in other oceans is as important as modelling that in the Pacific.

Because modes of SST variability outside the Pacific are in part forced by ENSO, simulation of SSTs outside the Pacific depends on model ability to reproduce not only ENSO SST variability, but also the relationship of ENSO with these modes, such as the IOD and the IOB. Models perform poorly in these simulations. For example, based on models of Phase 6 of the Coupled Model Intercomparison Project[117] (CMIP6), simulated amplitude of ENSO, the IOD and the IOB varies vastly across models (**Fig. 4a, b**). The amplitude of ENSO in individual models differs by a factor of five (x-axis, **Fig. 4a, b**), as seen in the matured season of DJF. A similar level of inter-model differences is seen in the amplitude of the IOD and the IOB (y-axis, **Fig. 4a, b**). Correspondingly, there is a strong inter-model difference in the relationship between ENSO and the IOD, or between ENSO and the IOB, or in simulated ENSO-induced rainfall (x-axis and y-axis, **Fig. 4c, d**).

However, the inter-model differences do reinforce the importance of the coupling between the Indian and Pacific Ocean SSTs in ENSO-induced rainfall over Africa. Models simulating a greater ENSO amplitude systematically produce a greater amplitude in the IOD or the IOB (**Fig. 4a, b**). More importantly, models simulating a greater ENSO-IOD coupling systematically produce a greater ENSO influence on rainfall over eastern Africa (**Fig. 4c, e**). Likewise, models that produce a greater

ENSO-IOB coupling systematically generate a greater rainfall response to ENSO, as shown in the dipole pattern over southern Africa (**Fig. 4d, f)**. The systematic influence is highlighted by spatial coherence in the influence via the IOD on east Africa and the dipole pattern in the influence on southern Africa (**Fig. 4e, 4f**). These inter-model relationships reinforce the importance of the inter-basin interaction that is difficult to simulate.

In part due to model inability to reproduce amplitude of ENSO SST variability, modes of SST variability within and outside the Pacific and their relationship with ENSO[15], many models simulate impacts that are weaker than the observed or are unable to simulate an observed impact completely. For example, only approximately 50% of models simulate a statistically significant correlation between rainfall in the northern tropical western Africa and ENSO (left panel, **Fig. 5a**). On the other hand, the simulated impact on southwestern southern Africa rainfall is overly strong in JAS, when an El Niño is associated with a negative SAM, inducing increased rainfall[54]. Models produce an impact on southern Africa summer rainfall concentrated over the western half (middle right panel, **Fig. 5a)**, rather than over the eastern half in observations.

Simulation of ENSO impacts on African climate is challenging also because ENSO impacts are modulated by multidecadal SST variability, which is however generally under-estimated in models. Multidecadal SST variability drives multidecadal rainfall variability[33,95,104,111], on which ENSO-induced rainfall anomalies superimpose. That such SST variability drives multidecadal rainfall variability has been attested by incorporating multidecadal SSTs in hindcast systems of African rainfall variability. The systems are able to reproduce the reduction of the Sahel rainfall from late 1960s and late 1980s, and the post-1980s recovery[33,118,119,120], supporting the dynamics that tropical SSTs relative to the subtropical North Atlantic determine the meridional moisture transport, convergence, and movement of rain-belt over the Sahel[33,95], and that the multi-decadal tropical Pacific and the Indian Ocean SSTs affect moisture convergence, vertical ascent, and the southern extent and course of the circulation excursion toward southern Africa[105]. However, the amplitude of rainfall variability is far smaller than that observed.

The multi-year rainfall predictability is in turn sourced from the AMV[121,122,123,124], the PDO[121,122,123,124], variability in the Indian Ocean and the Mediterranean Sea[33,120], and relative warming of the subtropical North Atlantic with respect to the tropics[125], although their relative importance is still under debate. However, for reasons still unknown, majority of models underestimate the amplitude of the IPO and the AMV[126,127,128,129].

5. Projected change in ENSO impact

Knowledge of how ENSO affects Africa climate has important implications for understanding and assessing projection of how the impact may change in the future. The assessment must include changes in the mean rainfall on which ENSO's impact superimposes, changes in ENSO-induced SST variability, or otherwise, within and outside the Pacific, and changes in extreme dry and wet conditions.

Projected mean rainfall changes

Under transient greenhouse warming, mean rainfall changes substantially (Supplementary Fig. 5), and features large inter-model differences. More than 80% of CMIP6 models project an increase in rainfall over the Central and Eastern Sahel[130,131,132,133,134,135,136,137], owing to several factors below. The Northern Hemisphere oceans warm faster than the Southern Hemisphere oceans[136,138] with an intensified north-minus-south SST gradient[139], favoring moisture convergence into the Northern Hemisphere[140]. The land-sea thermal contrast increases, intensifying the low-level West African Westerly Jet and moisture flux into the Sahel[130,132]. In addition, the Mediterranean warming enhances Sahel rainfall by inducing moisture convergence over the Sahel[141]. These processes support a projected overall Sahel rainfall increase; however, greenhouse warming-induced rise in tropical SSTs leads to a southward shift of the ITCZ, which by itself decreases rainfall in west Africa[132,135,142,143]. Thus, there is an east-west contrast in rainfall increase, weaker in the west, driven by an intensified Saharan Heat Low. The intensification increases south-westerly winds to Central and Eastern Sahel promoting rainfall there[136], but inhibits convection in the west Sahel[56,57].

Similarly, more than 80% of CMIP6 models project an increase in short rain over eastern Africa[144,145,146], consistent with a faster warming in the western equatorial Indian Ocean than in the eastern Indian Ocean[147,148,149]. Over southern Africa, rainfall is projected to decrease in JAS, SON and MAM, accompanied by a northward shift of the SICZ[150,151], a northward shift Congo Air Boundary[152], an expanding thermal low and a reduced number of tropical lows[152]. In the main rain season of DJF, there is a tendency for a slight rainfall increase but inter-model consensus on the change is low.

Projected change in SST variability.

Under transient greenhouse warming, majority of models project an increase in ENSO SST variability, translating into a projected increase in frequency of strong El Niño and strong La Niña events, swings from a strong El Niño to a strong La Niña event[78,91,153], and disproportionately more frequent multi-year La Niña events than those of strong El Niño events[154]. Strong pIOD events like the one in 2019 likely increase in frequency whereas moderate pIOD events decrease[148,149]. By contrast,

variability of Atlantic Niño/Niña is likely to decrease under greenhouse warming[155,156]. On interdecadal timescales, the PDO is projected to weaken in amplitude and to shorten in periodicity[157], whereas the AMV variance on multi-decadal time scales is projected to increase[158]. There is no systematic change in the relationship of ENSO with the IOD[141], nor with the IOB, the SIOD, the SASD, or the SAM in an analysis conducted for this review. Majority of models simulate a reduction in the relationship between ENSO and Atlantic Niño/Niña[159] as variability of Atlantic Niño/Niña decreases[155,156].

Projected increase in extreme anomalies.

Simulated ENSO's impact in all seasons is in general weaker than the observed[160], but the ENSO impacts from the 20th to the 21st century (**Fig. 5a, b**) show a general increase in all seasons. We measure ENSO impact in terms of rainfall sensitivity to ENSO SST anomalies. Over the Sahel, rainfall sensitivity intensifies and the area of ENSO impacts is enlarged, extending from a small area in the eastern region in the 20th century to the central and western portion in the 21th century (first column of **Fig. 5a, b**). The increased intensity and the enlarged area of impact are consistent with the projected increase in amplitude of ENSO variability, which increases the signal to noise ratio, leading to a greater response of rainfall to ENSO[76,78]. The enlarged area overlaps with the region of increased mean rainfall, increasing the capacity for wet and dry anomalies during La Niña and El Niño events, respectively.

Over East Africa, there is a similar increase in the sensitivity of equatorial East Africa short rain to ENSO, through the area of ENSO impact is little changed (second column of **Fig. 5a, b**). The intensified response is likewise due to the greater signal to noise ratio arising from increased ENSO amplitude given that there is no significant change in the ENSO-IOD relationship[149] and to the increased mean short rain (Supplementary Fig. 5) that facilitates a stronger response.

Over southern Africa, where the summer rainfall response to El Niño events features the dipole, an increased sensitivity and an enlarged area of the response over the wet pole region are projected (third column of **Fig. 5a, b**), due to the projected increase in ENSO amplitude and in mean rainfall. The greater sensitivity persists into the long-rain season over the equatorial eastern Africa (fourth column of **Fig. 5a, b**), where La Niña or multiyear La Niña induces droughts[32], despite little change in the mean rainfall over the region (Supplementary Fig. 5).

These changes, using all models, are reproduced using a subset of models that simulate a greater ENSO-IOD coupling or a stronger ENSO nonlinearity (Supplementary Figs 6 and 7). The small difference highlights the pivotal role of the

projected increase in ENSO variability in the 21st century. Because of the increased sensitivity and ENSO amplitude, frequency of both extreme dry and extreme wet anomalies surpassing a threshold value is generally higher in the 21st century (**Fig. 5, c-f**).

Over the Sahel, the frequency of extreme rainfall anomalies above the increasing trend is higher, translating into an increase of 63% and 135% in the number seasons with a negative and positive rainfall anomaly greater than a one-standard deviation value, respectively (**Fig. 5c**). In east Africa, the number of short rain seasons with a dry anomaly greater than a one-standard deviation value increases by 35% (**Fig. 5d**). there is a small increase in the wet seasons partly due to an offsetting effect from a decreased frequency of moderate positive IOD event coherent[148] with a non-extreme El Niño event. However, for strong El Niño events with an index larger than 1.75 s.d., the number of short rain seasons with a wet anomaly greater than a one-standard deviation value increases by 37%. Over southern Africa, the number of seasons with a dry and wet anomaly greater than the same threshold, increases by 10% and 47%, respectively (**Fig. 5e**), and long rain seasons over east Africa with a dry and wet anomaly increase by 53% and 20%, respectively (**Fig. 5f**).

6. Pathways forward

ENSO exerts a consequential impact on African climate by forcing anomalies in the tropical troposphere, driving tropical SST variability in the oceans neighbouring the continent, inducing extratropical oceanic and atmospheric anomalies, and changing regional circulations. The impact differs by ENSO events, and is asymmetric about El Niño and La Niña, and modulated by multidecadal variability. Modelling ENSO impact on Africa is challenging, because it involves simulating ENSO SST variability, its interaction with SST variability of other oceans, and their interactions with interdecadal variability. Under transient greenhouse warming, available models collectively suggest that ENSO-induced dry and wet anomalies are expected to increase over much of Africa, manifesting as an increased frequency of both dry and wet extremes. ENSO thus represents an important influence on African climate with profound impacts in a changing climate. Therefore, it is vital to reduce the uncertainties in our understanding of ENSO impact in contemporary and future climates, which can be achieved through continued model improvement and targeted research.

Climate models are an important tool for understanding past influence and projecting future impact from ENSO, but they suffer from long-standing systematic errors, including a cold bias in the equatorial central Pacific[161], overly strong easterly winds and overly cool SST in the equatorial eastern Indian Ocean[149,162], and a warm bias in

the eastern boundary current system regions of the tropical Pacific and Atlantic[115]. These biases have been found to have a substantial impact on the simulated characteristics of ENSO, the IOD, the Atlantic Niño/Niña and their interactions[15]. For example, the Pacific cold-tongue bias hinders establishment of atmosphere convection in the equatorial eastern Pacific, which is a key characteristic of extreme El Niño[78]; an atmospheric convection centre too far east due to the eastern Atlantic warm bias weakens feedback from the equatorial Atlantic to the Pacific, affecting ENSO periodicity, the IPO, and the Pacific mean state[15,115]. Strong biases also exist in the equatorial eastern Indian Ocean, leading to overly strong positive feedbacks, hence an overly high sensitivity of the IOD to stochastic forcing and an overly large IOD amplitude[149].

Impacts from some of the biases remain unknown. For example, it is not clear whether these biases lead to biases in simulated properties of African rainfall, namely, overly strong short rain that is higher than long rain[110,145], overly strong summer rainfall over southern Africa[160], a projected increase in east Africa annual rainfall[110,145], an overly weak ENSO-IOD coupling[149,160], or an overly weak ENSO impact on northern tropical western Africa, and an incorrect ENSO rainfall anomaly pattern over southern Africa. Thus, there remains considerable uncertainty in the projected change in ENSO impact on Africa.

Nevertheless, recent progress provides insightful guidance for setting research priorities. Addressing model systematic errors, particularly in the equatorial oceans, is urgent due to their potentially adverse impacts on ENSO and IOD properties, inter-basin interactions, and future projections. To capture detailed impacts from ENSO, particularly on regional circulation, higher spatial resolution might be necessary. For instance, the dynamics seen in the southern Africa rainfall dipole pattern involve not only ENSO and its inter-basin interactions but also regional processes that are not well simulated by global climate models[163]. In this regard, initiatives like internationally coordinated regional climate downscaling experiments (CORDEX) by the World Climate Research Programme[163] can be important. These coordinated regional climate downscaling experiments, utilizing global model outputs as boundary conditions, simulate regional processes crucial for extreme events[164,165,166], which are most consequential in terms of socio-economic impacts. However, inheriting biases from global models pose challenges[167]; for example, the bias in east Africa rainfall seasonality persists into regional models[164], emphasizing the need to rectify global model errors. Moreover, comprehensive studies are required to understand the interactions between climate change factors like high temperature, atmospheric moisture, and ENSO anomalies. Importantly, there is evidence

suggesting that climate change amplifies ENSO-related extreme events, for example, the severity of drought during the 2015-16 El Niño[168].

Progress in these areas will not only advance the science of ENSO, but also provide crucial inputs to policymaking aimed at mitigating its substantial impacts on African communities, often considered among the world's most vulnerable. Few other advances in ENSO research are as important as progress in comprehending, modelling and projecting ENSO impact on Africa, an area where strides can greatly benefit human society. Achieving such strides depends critically on a deeper understanding underpinned by continuous observations, comprehensive understanding, and improved modelling.

References

1 Goddard, L. & Graham, N. E. Importance of the Indian Ocean for simulating rainfall anomalies over eastern and southern Africa. *J. Geophys. Res.* **104**, 19099-19116 (1999).

2 Lindesay, J. A., Harrison, M. S. J. & Haffner, M. P. The southern oscillation and South African rainfall. *S. Afr. J. Sci.* **82**, 196-198 (1986).

3 Janicot, S., Moron, V. & Fontaine, B. Sahel droughts and ENSO dynamics. *Geophys. Res. Lett.* **23**, 515-518 (1996).

4 Rowell, D. P. Teleconnections between the tropical Pacific and the Sahel. *Q. J. R. Meteorol. Soc.* **127**, 1683-1706 (2001).

5 Giannini, A., Saravanan, R. & Chang, P. Oceanic forcing of Sahel rainfall on interannual to interdecadal time scales. *Science* **302**, 1027-1030 (2003).

6 Rodríguez-Fonseca, B. et al. Interannual and decadal SST-forced responses of the West African monsoon. *Atmos. Sci. Lett.* **12**, 67-74 (2011).

7 Rodríguez-Fonseca, B. et al. Variability and Predictability of West African Droughts: A Review on the Role of Sea Surface Temperature Anomalies. *J. Clim.* **28**, 4034-4060 (2015).

8 Nicholson, S. E. The West African Sahel: A Review of Recent Studies on the Rainfall Regime and Its Interannual Variability. *ISRN Meteorol.* **2013**, 1-32 (2013).

9 Nicholson, S. E. Climate and climatic variability of rainfall over eastern Africa. *Rev. Geophys.* **55**, 590-635 (2017).

10 Ropelewski, C. F. & Halpert, M. S. Global and Regional Scale Precipitation Patterns Associated with the El Niño/Southern Oscillation. *Mon. Wea. Rev.* **115**, 1606-1626 (1987).

11 Lintner, B. R. & Chiang, J. C. H. Reorganization of tropical climate during El Nino: A weak temperature gradient approach. *J. Clim.* **18**, 5312-5329 (2005).

12 de Oliveira, C. P., Aímola, L., Ambrizzi, T. & Freitas, A. C. V. The Influence of the Regional Hadley and Walker Circulations on Precipitation Patterns over Africa in El Niño, La Niña, and Neutral Years. *Pure Appl. Geophys.* **175**, 2293-2306 (2018).

13 Chang, P., Fang, Y., Saravanan, R., Ji, L. & Seidel, H. The cause of the fragile relationship between the Pacific El Nino and the Atlantic Nino. *Nature* **443**, 324-328 (2006).

14 Latif, M. & Grötzner, A. The equatorial Atlantic oscillation and its response to

ENSO. *Clim. Dyn.* **16**, 213-218 (2000).
15 Cai, W. et al. Pantropical climate interactions. *Science* **363**, eaav4236 (2019).
16 Halpern, D. & Woiceshyn, P. M. Somali Jet in the Arabian Sea, El Niño, and India Rainfall. *J. Clim.* **14**, 434-441 (2001).
17 Riddle, E. E. & Cook, K. H. Abrupt rainfall transitions over the Greater Horn of Africa: Observations and regional model simulations. *J. Geophys. Res.* **113**, D15109 (2008).
18 Howard, E. & Washington, R. Characterizing the Synoptic Expression of the Angola Low. *J. Clim.* **31**, 7147-7165 (2018).
19 Blamey, R. C., Kolusu, S. R., Mahlalela, P., Todd, M. C. & Reason, C. J. C. The role of regional circulation features in regulating El Nino climate impacts over southern Africa: A comparison of the 2015/2016 drought with previous events. *Int. J. Climatol.* **38**, 4276-4295 (2018).
20 Cook, K. H. The South Indian convergence zone and interannual rainfall variability over southern Africa. *J. Clim.* **13**, 3789-3804 (2000).
21 Pu, B. & Cook, K. H. Dynamics of the West African Westerly Jet. *J. Clim.* **23**, 6263-6276 (2010).
22 Cook, K. H. Generation of the African easterly jet and its role in determining West African precipitation. *J. Clim.* **12**, 1165-1184 (1999).
23 Viste, E. & Sorteberg, A. Moisture transport into the Ethiopian highlands. *Int. J. Climatol.* **33**, 249-263 (2013).
24 Howard, E. & Washington, R. Drylines in Southern Africa: Rediscovering the Congo Air Boundary. *J. Clim.* **32**, 8223-8242 (2019).
25 Yang, W., Seager, R., Cane, M. A. & Lyon, B. The Annual Cycle of East African Precipitation. *J. Clim.* **28**, 2385-2404 (2015).
26 Hart, N. C. G., Reason, C. J. C. & Fauchereau, N. Cloud bands over southern Africa: seasonality, contribution to rainfall variability and modulation by the MJO. *Clim. Dyn.* **41**, 1199-1212 (2013).
27 Harrison, M. S. J. A generalized classification of South African summer rain-bearing synoptic systems. *J. Climatol.* **4**, 547-560 (1984).
28 Macron, C., Pohl, B., Richard, Y. & Bessafi, M. How do Tropical Temperate Troughs Form and Develop over Southern Africa? *J. Clim.* **27**, 1633-1647 (2014).
29 Reason, C. J. C. The Bolivian, Botswana, and Bilybara Highs and Southern Hemisphere drought/floods. *Geophys. Res. Lett.* **43**, 1280-1286 (2016).
30 FEWS NET. Already unprecedented food assistance needs grow further; risk of Famine persists. (2017).
31 Kimutai, J. B., C; Zachariah, M; Philip, S; Kew, S; Pinto, I; Wolski, P; Koren, G; Vecchi, G; Yang, W; Li, S; Vahlberg, M; Singh, R; Heinrich, D; Pereira, CM; Arrighi, J; Thalheimer, L; Kane, C; Otto, FEL. Human-induced climate change increased drought severity in Horn of Africa. https://doi.org/10.25561/103482 (2023).
32 Funk, C. et al. Examining the role of unusually warm Indo-Pacific sea-surface temperatures in recent African droughts. *Q. J. R. Meteorol. Soc.* **144**, 360-383 (2018).
33 Sheen, K. L. et al. Skilful prediction of Sahel summer rainfall on inter-annual and multi-year timescales. *Nat. Commun.* **8**, 1-12 (2017).
34 Gleixner, S., Keenlyside, N., Viste, E. & Korecha, D. The El Niño effect on Ethiopian summer rainfall. *Clim. Dyn.* **49**, 1865-1883 (2017).
35 Diro, G. T., Grimes, D. I. F. & Black, E. Teleconnections between Ethiopian

summer rainfall and sea surface temperature: part I—observation and modelling. *Clim. Dyn.* **37**, 103-119 (2011).
36 Janicot, S., Trzaska, S. & Poccard, I. Summer Sahel-ENSO teleconnection and decadal time scale SST variations. *Clim. Dyn.* **18**, 303-320 (2001).
37 Joly, M. & Voldoire, A. Influence of ENSO on the West African Monsoon: Temporal Aspects and Atmospheric Processes. *J. Clim.* **22**, 3193-3210 (2009).
38 Saji, N. H., Goswami, B. N., Vinayachandran, P. N. & Yamagata, T. A dipole mode in the tropical Indian Ocean. *Nature* **401**, 360-363 (1999).
39 Weller, E. et al. More-frequent extreme northward shifts of eastern Indian Ocean tropical convergence under greenhouse warming. *Sci. Rep.* **4**, 6087 (2014).
40 Black, E., Slingo, J. & Sperber, K. R. An observational study of the relationship between excessively strong short rains in coastal East Africa and Indian Ocean SST. *Mon. Wea. Rev.* **131**, 74-94 (2003).
41 Moihamette, F., Pokam, W. M., Diallo, I. & Washington, R. Extreme Indian Ocean dipole and rainfall variability over Central Africa. *Int. J. Climatol.* **42**, 5255-5272 (2022).
42 Klein, S. A., Soden, B. J. & Lau, N. C. Remote sea surface temperature variations during ENSO: Evidence for a tropical atmospheric bridge. *J. Clim.* **12**, 917-932 (1999).
43 Hart, N. C. G., Washington, R. & Reason, C. J. C. On the Likelihood of Tropical-Extratropical Cloud Bands in the South Indian Convergence Zone during ENSO Events. *J. Clim.* **31**, 2797-2817 (2018).
44 Barimalala, R., Blamey, R. C., Desbiolles, F. & Reason, C. J. C. Variability in the Mozambique Channel Trough and Impacts on Southeast African Rainfall. *J. Clim.* **33**, 749-765 (2020).
45 Reason, C. J. C. Subtropical Indian Ocean SST dipole events and southern African rainfall. *Geophys. Res. Lett.* **28**, 2225-2227 (2001).
46 Behera, S. K. & Yamagata, T. Subtropical SST dipole events in the southern Indian ocean. *Geophys. Res. Lett.* **28**, 327-330 (2001).
47 Fauchereau, N., Trzaska, S., Richard, Y., Roucou, P. & Camberlin, P. Sea-surface temperature co-variability in the southern Atlantic and Indian Oceans and its connections with the atmospheric circulation in the southern hemisphere. *Int. J. Climatol.* **23**, 663-677 (2003).
48 Palmer, P. I. et al. Drivers and impacts of Eastern African rainfall variability. *Nat. Rev. Earth Environ.* **4**, 254-270 (2023).
49 Xie, S. P. & Carton, J. A. Tropical Atlantic Variability: Patterns, Mechanisms, and Impacts. *Am. Geophys. Union* **147**, 121-42 (2004).
50 Pomposi, C., Giannini, A., Kushnir, Y. & Lee, D. E. Understanding Pacific Ocean influence on interannual precipitation variability in the Sahel. *Geophys. Res. Lett.* **43**, 9234-9242 (2016).
51 Rowell, D. P. The impact of Mediterranean SSTs on the Sahelian rainfall season. *J. Clim.* **16**, 849-862 (2003).
52 Fontaine, B. et al. Impacts of warm and cold situations in the Mediterranean basins on the West African monsoon: observed connection patterns (1979-2006) and climate simulations. *Clim. Dyn.* **35**, 95-114 (2010).
53 Thompson, D. W. J. & Wallace, J. M. Annular modes in the extratropical circulation. Part I: Month-to-month variability. *J. Clim.* **13**, 1000-1016 (2000).
54 Reason, C. J. C. & Rouault, M. Links between the Antarctic Oscillation and winter rainfall over western South Africa. *Geophys. Res. Lett.* **32**, L07705 (2005).
55 Mahlalela, P. T., Blamey, R. C., Hart, N. C. G. & Reason, C. J. C. Drought in the

Eastern Cape region of South Africa and trends in rainfall characteristics. *Clim. Dyn.* **55**, 2743-2759 (2020).
56 Lavaysse, C., Flamant, C. & Janicot, S. Regional-scale convection patterns during strong and weak phases of the Saharan heat low. *Atmos. Sci. Lett.* **11**, 255-264 (2010).
57 Lavaysse, C., Flamant, C., Evan, A., Janicot, S. & Gaetani, M. Recent climatological trend of the Saharan heat low and its impact on the West African climate. *Clim. Dyn.* **47**, 3479-3498 (2016).
58 Thorncroft, C. D. & Blackburn, M. Maintenance of the African easterly jet. *Q. J. R. Meteorol. Soc.* **125**, 763-786 (1999).
59 Iqbal, W. et al. Mean climate and representation of jet streams in the CORDEX South Asia simulations by the regional climate model RCA4. *Theor. Appl. Climatol.* **129**, 1-19 (2017).
60 Vizy, E. K. & Cook, K. H. Connections between the summer east African and Indian rainfall regimes. *J. Geophys. Res.* **108**, 4510 (2003).
61 Jain, S., Mishra, S. K., Anand, A., Salunke, P. & Fasullo, J. T. Historical and projected low-frequency variability in the Somali Jet and Indian Summer Monsoon. *Clim. Dyn.* **56**, 749-765 (2021).
62 Crétat, J., Pohl, B., Dieppois, B., Berthou, S. & Pergaud, J. The Angola Low: relationship with southern African rainfall and ENSO. *Clim. Dyn.* **52**, 1783-1803 (2019).
63 Reason, C. J. C. et al. A review of South African research in atmospheric science and physical oceanography during 2000-2005 : review article. *S. Afr. J. Sci.* **102**, 35-45 (2006).
64 Todd, M. & Washington, R. Circulation anomalies associated with tropical-temperate troughs in southern Africa and the south west Indian Ocean. *Clim. Dyn.* **15**, 937-951 (1999).
65 Pohl, B., Fauchereau, N., Richard, Y., Rouault, M. & Reason, C. J. C. Interactions between synoptic, intraseasonal and interannual convective variability over Southern Africa. *Clim. Dyn.* **33**, 1033-1050 (2009).
66 Manhique, A. J., Reason, C. J. C., Rydberg, L. & Fauchereau, N. ENSO and Indian Ocean sea surface temperatures and their relationships with tropical temperate troughs over Mozambique and the Southwest Indian Ocean. *Int. J. Climatol.* **31**, 1-13 (2011).
67 Hart, N. C. G., Reason, C. J. C. & Fauchereau, N. Tropical–Extratropical Interactions over Southern Africa: Three Cases of Heavy Summer Season Rainfall. *Mon. Wea. Rev.* **138**, 2608-2623 (2010).
68 Lazenby, M. J., Todd, M. C. & Wang, Y. Climate model simulation of the South Indian Ocean Convergence Zone: mean state and variability. *Clim. Res.* **68**, 59-71 (2016).
69 Barimalala, R., Desbiolles, F., Blamey, R. C. & Reason, C. Madagascar Influence on the South Indian Ocean Convergence Zone, the Mozambique Channel Trough and Southern African Rainfall. *Geophys. Res. Lett.* **45**, 11,380-311,389 (2018).
70 Driver, P. & Reason, C. J. C. Variability in the Botswana High and its relationships with rainfall and temperature characteristics over southern Africa. *Int. J. Climatol.* **37**, 570-581 (2017).
71 Maoyi, M. L. & Abiodun, B. J. How well does MPAS-atmosphere simulate the characteristics of the Botswana High? *Clim. Dyn.* **57**, 2109-2128 (2021).
72 Bader, J. & Latif, M. The 1983 drought in the West Sahel: a case study. *Clim. Dyn.* **36**, 463-472 (2011).

73 Kug, J. S., Jin, F. F. & An, S.-I. Two Types of El Niño Events: Cold Tongue El Niño and Warm Pool El Niño. *J. Clim.* **22**, 1499-1515 (2009).
74 Takahashi, K., Montecinos, A., Goubanova, K. & Dewitte, B. ENSO regimes: Reinterpreting the canonical and Modoki El Niño. *Geophys. Res. Lett.* **38** (2011).
75 Capotondi, A. et al. Understanding ENSO Diversity. *Bull. Am. Meteorol. Soc.* **96**, 921-938 (2015).
76 Cai, W. et al. ENSO and greenhouse warming. *Nat. Clim. Change* **5**, 849-859 (2015).
77 Cai, W. et al. Increased variability of eastern Pacific El Niño under greenhouse warming. *Nature* **564**, 201-206 (2018).
78 Cai, W. et al. Changing El Nino-Southern Oscillation in a warming climate. *Nat. Rev. Earth Environ.* **2**, 628-644 (2021).
79 Frauen, C., Dommenget, D., Tyrrell, N., Rezny, M. & Wales, S. Analysis of the Nonlinearity of El Niño–Southern Oscillation Teleconnections. *J. Clim.* **27**, 6225-6244 (2014).
80 Cai, W. et al. Increased frequency of extreme La Niña events under greenhouse warming. *Nat. Clim. Change* **5**, 132-137 (2015).
81 Takahashi, K. & Dewitte, B. Strong and moderate nonlinear El Niño regimes. *Clim. Dyn.* **46**, 1627-1645 (2016).
82 Ashok, K., Behera, S. K., Rao, S. A., Weng, H. & Yamagata, T. El Niño Modoki and its possible teleconnection. *J. Geophys. Res.* **112**, C11007 (2007).
83 Ratnam, J. V., Behera, S. K., Masumoto, Y. & Yamagata, T. Remote Effects of El Niño and Modoki Events on the Austral Summer Precipitation of Southern Africa. *J. Clim.* **27**, 3802-3815 (2014).
84 Preethi, B., Sabin, T. P., Adedoyin, J. A. & Ashok, K. Impacts of the ENSO Modoki and other Tropical Indo-Pacific Climate-Drivers on African Rainfall. *Sci. Rep.* **5**, 16653 (2015).
85 Jia, F., Cai, W., Gan, B., Wu, L. & Di Lorenzo, E. Enhanced North Pacific impact on El Niño/Southern Oscillation under greenhouse warming. *Nat. Clim. Change* **11**, 840-847 (2021).
86 Cai, W. et al. Increasing frequency of extreme El Niño events due to greenhouse warming. *Nat. Clim. Change* **4**, 111-116 (2014). Should be extreme IOD
87 Richard, Y., Trzaska, S., Roucou, P. & Rouault, M. Modification of the southern African rainfall variability/ENSO relationship since the late 1960s. *Clim. Dyn.* **16**, 883-895 (2000).
88 Clark, C. O., Webster, P. J. & Cole, J. E. Interdecadal variability of the relationship between the Indian Ocean zonal mode and East African coastal rainfall anomalies. *J. Clim.* **16**, 548-554 (2003).
89 Suárez-Moreno, R., Rodríguez-Fonseca, B., Barroso, J. A. & Fink, A. H. Interdecadal Changes in the Leading Ocean Forcing of Sahelian Rainfall Interannual Variability: Atmospheric Dynamics and Role of Multidecadal SST Background. *J. Clim.* **31**, 6687-6710 (2018).
90 Kim, S., Cai, W., Jin, FF. *et al.* Response of El Niño sea surface temperature variability to greenhouse warming. *Nature Clim Change* **4**, 786–790 (2014). https://doi.org/10.1038/nclimate2326.
91 Cai, W. et al. Anthropogenic impacts on twentieth-century ENSO variability changes. *Nat. Rev. Earth Environ.* **4**, 407-418 (2023).
92 Pomposi, C., Kushnir, Y., Giannini, A. & Biasutti, M. Toward Understanding the Occurrence of Both Wet and Dry Sahel Seasons during El Nino: The Modulating Role of the Global Ocean. *J. Clim.* **33**, 1193-1207 (2020).

93 Ham, Y. G., Kug, J. S. & Park, J. Y. Two distinct roles of Atlantic SSTs in ENSO variability: North Tropical Atlantic SST and Atlantic Nino. *Geophys. Res. Lett.* **40**, 4012-4017 (2013).
94 Nnamchi, H. C., Dike, V. N., Akinsanola, A. A. & Okoro, U. K. Leading patterns of the satellite-era summer precipitation over West Africa and associated global teleconnections. *Atmos. Res.* **259**, 105677 (2021).
95 Mohino, E., Janicot, S. & Bader, J. Sahel rainfall and decadal to multi-decadal sea surface temperature variability. *Clim. Dyn.* **37**, 419-440 (2011).
96 Losada, T. et al. Tropical SST and Sahel rainfall: A non-stationary relationship. *Geophys. Res. Lett.* **39**, L12705 (2012).
97 Ashok, K., Guan, Z. Y. & Yamagata, T. A look at the relationship between the ENSO and the Indian Ocean Dipole. *J. Meteor. Soc. Japan* **81**, 41-56 (2003).
98 Kebacho, L. L. Large-scale circulations associated with recent interannual variability of the short rains over East Africa. *Meteorol. Atmos. Phys.* **134**, 10 (2022).
99 Ham, Y. G., Choi, J. Y. & Kug, J. S. The weakening of the ENSO-Indian Ocean Dipole (IOD) coupling strength in recent decades. *Clim. Dyn.* **49**, 249-261 (2017).
100 Manatsa, D., Mukwada, G. & Makaba, L. ENSO shifts and their link to Southern Africa surface air temperature in summer. *Theor. Appl. Climatol.* **132**, 727-738 (2018).
101 Manatsa, D. & Matarira, C. H. Changing dependence of Zimbabwean rainfall variability on ENSO and the Indian Ocean dipole/zonal mode. *Theor. Appl. Climatol.* **98**, 375-396 (2009).
102 Hoell, A., Funk, C., Zinke, J. & Harrison, L. Modulation of the Southern Africa precipitation response to the El Niño Southern Oscillation by the subtropical Indian Ocean Dipole. *Clim. Dyn.* **48**, 2529-2540 (2017).
103 Wang, S. S., Huang, J. P., He, Y. L. & Guan, Y. P. Combined effects of the Pacific Decadal Oscillation and El Nino-Southern Oscillation on Global Land Dry-Wet Changes. *Sci. Rep.* **4**, 6651 (2014).
104 Villamayor, J. & Mohino, E. Robust Sahel drought due to the Interdecadal Pacific Oscillation in CMIP5 simulations. *Geophys. Res. Lett.* **42**, 1214-1222 (2015).
105 Mason, S. J. El Nino, climate change, and Southern African climate. *Environ.* **12**, 327-345 (2001).
106 Malherbe, J., Dieppois, B., Maluleke, P., Van Staden, M. & Pillay, D. L. South African droughts and decadal variability. *Nat. Hazards* **80**, 657-681 (2016).
107 Yang, W. C., Seager, R., Cane, M. A. & Lyon, B. The East African Long Rains in Observations and Models. *J. Clim.* **27**, 7185-7202 (2014).
108 Lyon, B. Seasonal Drought in the Greater Horn of Africa and Its Recent Increase during the March May Long Rains. *J. Clim.* **27**, 7953-7975 (2014).
109 Liebmann, B. et al. Climatology and Interannual Variability of Boreal Spring Wet Season Precipitation in the Eastern Horn of Africa and Implications for Its Recent Decline. *J. Clim.* **30**, 3867-3886 (2017).
110 Funk, C. et al. Warming of the Indian Ocean threatens eastern and southern African food security but could be mitigated by agricultural development. *P. Natl. Acad. Sci. USA* **105**, 11081-11086 (2008).
111 Hoerling, M., Hurrell, J., Eischeid, J. & Phillips, A. Detection and Attribution of Twentieth-Century Northern and Southern African Rainfall Change. *J. Clim.* **19**, 3989-4008 (2006).
112 Zhang, R. & Delworth, T. L. Impact of Atlantic multidecadal oscillations on

India/Sahel rainfall and Atlantic hurricanes. *Geophys. Res. Lett.* **33**, L17712 (2006).
113 Badji, A., Mohino, E., Diakhate, M., Mignot, J. & Gaye, A. T. Decadal Variability of Rainfall in Senegal: Beyond the Total Seasonal Amount. *J. Clim.* **35**, 5339-5358 (2022).
114 Ruprich-Robert, Y. et al. Assessing the Climate Impacts of the Observed Atlantic Multidecadal Variability Using the GFDL CM2.1 and NCAR CESM1 Global Coupled Models. *J. Clim.* **30**, 2785-2810 (2017).
115 McGregor, S. et al. Recent Walker circulation strengthening and Pacific cooling amplified by Atlantic warming. *Nat. Clim. Change* **4**, 888-892 (2014).
116 Li, X. C., Xie, S. P., Gille, S. T. & Yoo, C. Atlantic-induced pan-tropical climate change over the past three decades. *Nat. Clim. Change* **6**, 275-279 (2016).
117 Eyring, V. et al. Overview of the Coupled Model Intercomparison Project Phase 6 (CMIP6) experimental design and organization. *Geosci. Model Dev.* **9**, 1937-1958 (2016).
118 Zanna, L. Forecast Skill and Predictability of Observed Atlantic Sea Surface Temperatures. *J. Clim.* **25**, 5047-5056 (2012).
119 Yeager, S. G. et al. PREDICTING NEAR-TERM CHANGES IN THE EARTH SYSTEM A Large Ensemble of Initialized Decadal Prediction Simulations Using the Community Earth System Model. *Bull. Am. Meteorol. Soc.* **99**, 1867-1886 (2018).
120 He, Y. J. et al. Role of Ocean Initialization in Skillful Prediction of Sahel Rainfall on the Decadal Time Scale. *J. Clim.* **36**, 2109-2129 (2023).
121 Mohino, E., Keenlyside, N. & Pohlmann, H. Decadal prediction of Sahel rainfall: where does the skill (or lack thereof) come from? *Clim. Dyn.* **47**, 3593-3612 (2016).
122 Gaetani, M. & Mohino, E. Decadal Prediction of the Sahelian Precipitation in CMIP5 Simulations. *J. Clim.* **26**, 7708-7719 (2013).
123 García-Serrano, J., Guemas, V. & Doblas-Reyes, F. J. Added-value from initialization in predictions of Atlantic multi-decadal variability. *Clim. Dyn.* **44**, 2539-2555 (2015).
124 Bellucci, A. et al. An assessment of a multi-model ensemble of decadal climate predictions. *Clim. Dyn.* **44**, 2787-2806 (2015).
125 Martin, E. R. & Thorncroft, C. Sahel rainfall in multimodel CMIP5 decadal hindcasts. *Geophys. Res. Lett.* **41**, 2169-2175 (2014).
126 Du, Y. and H. Chen Evaluation of CMIP6 model performance in simulating the PDO and its future change. Atmospheric and Oceanic Science Letters 17 (2024) 100449.
127 Xu, Y., T. Li, M. Xu, S. Shen, Z. Hu. Evaluation of the Pacific Decadal Oscillationfrom 1901 to 2014 in CMlP6 models, Clim Res 90:1-15 (2023). https://doi.org/10.3354/cr01711
128 Ma, Y., Yuan, N., Dong, T. et al. On the Pacific Decadal Oscillation Simulations in CMIP6 Models: A New Test-Bed from Climate Network Analysis. Asia-Pac J Atmos Sci 59, 17–28 (2023). https://doi.org/10.1007/s13143-022-00286-1
129 Li, S. et al. Increased Atlantic multidecadal climate variability under persistent greenhouse warming (2025 in press)
130 Haarsma, R. J., Selten, F. M., Weber, S. L. & Kliphuis, M. Sahel rainfall variability and response to greenhouse warming. *Geophys. Res. Lett.* **32**, L17702 (2005).
131 Monerie, P.-A., Fontaine, B., & Roucou, P. Expected future changes in the

African monsoon between 2030 and 2070 using some CMIP3 and CMIP5 models under a medium‐low RCP scenario. *J. Geophys. Res.* **117,** D16111 (2012).
132 Vizy, E. K., Cook, K. H., Crétat, J. & Neupane, N. Projections of a Wetter Sahel in the Twenty-First Century from Global and Regional Models. *J. Clim.* **26**, 4664-4687 (2013).
133 Akinsanola, A. A., & Zhou, W. Ensemble-based CMIP5 simulations of West African summer monsoon rainfall: current climate and future changes. *Theor. Appl. Climatol.* **136,** 1021-1031 (2019).
134 Almazroui, M. et al. Projected change in temperature and precipitation over Africa from CMIP6. *Earth Syst. Environ.* **4**, 455-475 (2020).
135 Monerie, P.-A., Sanchez-Gomez, E., Gaetani, M., Mohino, E. & Dong, B. Future evolution of the Sahel precipitation zonal contrast in CESM1. *Clim. Dyn.* **55**, 2801-2821 (2020).
136 Monerie, P. A., Pohl, B., & Gaetani, M. The fast response of Sahel precipitation to climate change allows effective mitigation action. *npj Clim. Atmos. Sci.* **4**, 24 (2021).
137 Zhang, Z., & Li, G. Uncertainty in the projected changes of Sahel summer rainfall under global warming in CMIP5 and CMIP6 multi-model ensembles. *Clim. Dyn.* **59**, 3579-3597 (2022).
138 Cai, W. et al. Southern Ocean warming and its climatic impacts. *Sci. Bull.* **68**, 946-960 (2023).
139 IPCC. *Climate Change 2021: The Physical Science Basis. Contribution of Working Group I to the Sixth Assessment Report of the Intergovernmental Panel on Climate Change* [Masson-Delmotte .V, P. Zhai, A. Pirani, S.L. Connors, C. Péan, S. Berger, N. Caud, Y. Chen, L. Goldfarb, M.I. Gomis, M. Huang, K. Leitzell, E. Lonnoy, J.B.R. Matthews, T.K. Maycock, T. Waterfield, O. Yelekçi, R. Yu, and B. Zhou (eds.)] (Cambridge University Press, 2021)
140 Guilbert, M., Terray, P., Mignot, J., Ollier, L. & Gastineau, G. Interhemispheric Temperature Gradient and Equatorial Pacific SSTs Drive Sahel Monsoon Uncertainties under Global Warming. *J. Clim.* **37**, 1033-1052 (2024).
141 Park, J.-y., Bader, J. & Matei, D. Anthropogenic Mediterranean warming essential driver for present and future Sahel rainfall. *Nat. Clim. Change* **6**, 941-945 (2016).
142 Gaetani, M. et al. West African monsoon dynamics and precipitation: the competition between global SST warming and CO2 increase in CMIP5 idealized simulations. *Clim. Dyn.* **48**, 1353-1373 (2017).
143 Paeth, H. & Hense, A. SST versus Climate Change Signals in West African Rainfall: 20th-Century Variations and Future Projections. *Clim. Change* **65**, 179-208 (2004).
144 Shongwe, M. E., van Oldenborgh, G. J., van den Hurk, B. & van Aalst, M. Projected Changes in Mean and Extreme Precipitation in Africa under Global Warming. Part II: East Africa. *J. Clim.* **24**, 3718-3733 (2011).
145 Tierney, J. E., Ummenhofer, C. C. & deMenocal, P. B. Past and future rainfall in the Horn of Africa. *Sci. Adv.* **1**, e1500682 (2015).
146 Wainwright, C. M. et al. 'Eastern African Paradox' rainfall decline due to shorter not less intense Long Rains. *npj Clim. Atmos. Sci.* **2**, 34 (2019).
147 Cai, W. et al. Projected response of the Indian Ocean Dipole to greenhouse warming. *Nat. Geosci.* **6**, 999-1007 (2013).
148 Cai, W. et al. Opposite response of strong and moderate positive Indian Ocean Dipole to global warming. *Nat. Clim. Change* **11**, 27-32 (2021).

149 Wang, G. Changing Indian Ocean Dipole in a warming climate. *Nat. Rev. Earth Environ.* (2024), in press.
150 Munday, C. & Washington, R. Controls on the Diversity in Climate Model Projections of Early Summer Drying over Southern Africa. *J. Clim.* **32**, 3707-3725 (2019).
151 Lazenby, M. & Todd, M. Evaluating future changes in the South Indian Ocean Convergence Zone projected by CMIP5 models and associated uncertainty. *Clim. Res.* **91**, 191-209 (2023).
152 Howard, E. & Washington, R. Tracing Future Spring and Summer Drying in Southern Africa to Tropical Lows and the Congo Air Boundary. *J. Clim.* **33**, 6205-6228 (2020).
153 Cai, W. et al. Increased ENSO sea surface temperature variability under four IPCC emission scenarios. *Nat. Clim. Change* **12**, 228-231 (2022).
154 Geng, T. et al. Increased occurrences of consecutive La Nina events under global warming. *Nature* **619**, 774-781 (2023).
155 Crespo, L. R. et al. Weakening of the Atlantic Nino variability under global warming. *Nat. Clim. Change* **12**, 822-827 (2022).
156 Yang, Y. et al. Suppressed Atlantic Nino/Nina variability under greenhouse warming. *Nat. Clim. Change* **12**, 814-821 (2022).
157 Li, S. J. et al. The Pacific Decadal Oscillation less predictable under greenhouse warming. *Nat. Clim. Change* **10**, 30-34 (2020).
158 Li, S. Increase variability of Atlantic Multi-decadal variability under greenhouse warming. *Nat. Clim. Change* (2024), in press.
159 Jia, F. et al. Weakening Atlantic Niño-Pacific connection under greenhouse warming. *Sci. Adv.* **5**, eaax4111 (2019).
160 Dieppois, B., Rouault, M. & New, M. The impact of ENSO on Southern African rainfall in CMIP5 ocean atmosphere coupled climate models. *Clim. Dyn.* **45**, 2425-2442 (2015).
161 Li, G. & Xie, S. P. Tropical Biases in CMIP5 Multimodel Ensemble: The Excessive Equatorial Pacific Cold Tongue and Double ITCZ Problems. *J. Clim.* **27**, 1765-1780 (2014).
162 Hirons, L. & Turner, A. The Impact of Indian Ocean Mean-State Biases in Climate Models on the Representation of the East African Short Rains. *J. Clim.* **31**, 6611-6631 (2018).
163 Giorgi, F., Jones, C. & Asrar, G. R. Addressing climate information needs at the regional level: the CORDEX framework. *WMO Bull.* **58**, 175-183 (2009).
164 Endris, H. S. et al. Assessment of the Performance of CORDEX Regional Climate Models in Simulating East African Rainfall. *J. Clim.* **26**, 8453-8475 (2013).
165 Engelbrecht, F. et al. Multi-scale climate modelling over Southern Africa using a variable-resolution global model. *Water Sa* **37**, 647-658 (2011).
166 Dosio, A. & Panitz, H.-J. Climate change projections for CORDEX-Africa with COSMO-CLM regional climate model and differences with the driving global climate models. *Clim. Dyn.* **46**, 1599-1625 (2016).
167 Hong, S. Y. & Kanamitsu, M. Dynamical downscaling: Fundamental issues from an NWP point of view and recommendations. *Asia-Pac. J. Atmos. Sci.* **50**, 83-104 (2014).
168 Funk, C. in *Drought, Flood, Fire: How Climate Change Contributes to Catastrophes* (ed. Chris C. Funk) 186-211 (Cambridge University Press, 2021).
169 Harris, I., Osborn, T. J., Jones, P. & Lister, D. Version 4 of the CRU TS monthly

high-resolution gridded multivariate climate dataset. *Sci. Data* **7**, 109 (2020).
170 Hersbach, H. et al. The ERA5 global reanalysis. *Q. J. R. Meteorol. Soc.* **146**, 1999-2049 (2020).
171 Kalnay, E. et al. The NCEP/NCAR 40-Year Reanalysis Project. *Bull. Am. Meteorol. Soc.* **77**, 437-472 (1996).
172 Schneider, U., Fuchs, T., Meyer-Christoffer, A. & Rudolf, B. Global Precipitation Analysis Products of the GPCC. *Global Precipitation Climatology Centre (GPCC), DWD, Internet Publikation,* **112**, 3819-3837 (2008).
173 Huang, B. et al. Extended Reconstructed Sea Surface Temperature, Version 5 (ERSSTv5): Upgrades, Validations, and Intercomparisons. *J. Clim.* **30**, 8179-8205 (2017).
174 Rayner, N. A. et al. Global analyses of sea surface temperature, sea ice, and night marine air temperature since the late nineteenth century. *J. Geophys. Res.* **108** (2003).
175 Huang, B. et al. Improvements of the Daily Optimum Interpolation Sea Surface Temperature (DOISST) Version 2.1. *J. Clim.* **34**, 2923-2939 (2021).
176 Henley, B. J. et al. A Tripole Index for the Interdecadal Pacific Oscillation. *Clim. Dyn.* **45**, 3077-3090 (2015).
177 Deser, C. & Phillips, A. S. Defining the Internal Component of Atlantic Multidecadal Variability in a Changing Climate. *Geophys. Res. Lett.* **48**, e2021GL095023 (2021).
178 Reynolds, R. W., Rayner, N. A., Smith, T. M., Stokes, D. C. & Wang, W. An Improved In Situ and Satellite SST Analysis for Climate. *J. Clim.* **15**, 1609-1625 (2002).

Box 1: African seasonal circulation

African seasonal climate varies vastly by regions. In mid-May, monsoonal rain reaches west Africa 5°N[8], and the cross-equatorial branch of the Somali Jet starts to bring moisture and rainfall northward to the southern slopes of the Ethiopian plateau. Toward June, Saharan Heat Low establishes, and the equatorial Atlantic cold tongue develops, facilitating summer southwesterlies that extend rain belt to its northernmost location 10°N by August[7,8] (**Box Fig. 1a**). In July, August, and September (JAS), in which the Sahel region receives 80% of its annual rainfall[27] (**Box Fig. 1b**), cyclonic circulation associated with Saharan Heat Low (blue circle) connects southwesterly monsoonal flows to the south and the northeasterly to the east from the Mediterranean region (red arrows, **Box Fig. 1a**). Sahelian surface ascent peaks at the West African coast, just east of the onshore West African Westerly Jet[21], which, together with African Easterly Jet around 600 hPa at 15°N and Tropical Easterly Jet around 200 hPa at 5°N, form a two-celled vertical circulation[8,22]. The tropical rain belt centres around 10°N, south of the Intertropical Convergence Zone[8] (ITCZ) at ~17°N. The Indian Ocean subtropical high pressure is at its northern-most latitudes, and moisture influx from sources including the Congo basin, the Red Sea, and the Indian Ocean through the Somali Jet (**thick** red arrow, **Box Fig. 1a**), results in high rainfall over northern East Africa[9,23].

During September, October, and November (SON), the tropical rain belt shifts southward. The Angola Low operates as a mixture of dry heat low and moist tropical

low. A dryline develops featuring well-defined wind convergence and humidity gradients, referred to as Congo Air Boundary[24]. From October to early December (OND), onset of onshore moisture transport from the Indian Ocean drives coastal and topographic uplifts in the western highlands producing "short rain" season[1,25] in east Africa countries (**Box Fig. 1c**).

During December, January and February (DJF), northeast trade winds blow across the northwest Indian Ocean and strong westerlies prevail over the equatorial Indian Ocean[1]. The subtropical Indian and Atlantic high-pressure systems are at their southern-most latitudes, facilitating convergence of winds into southern Africa (red arrows **Box Fig. 1d**), producing a peak season of rainfall (**Box Fig. 1e**). These winds include north-westerlies from the tropical Atlantic picking up moisture from the Congo basin, easterlies from the southwest Indian Ocean and northeasterlies from the equatorial western Indian Ocean carrying moisture from the warm Indian Ocean. The convergence, uplift and instability, together with the upper-level divergence of the leading edge of midlatitude westerly troughs, support development of tropical–extratropical cloud-band events[26], known as Tropical Temperate Troughs (white cloud **Box Fig. 1d)**. The troughs accompany development of tropical low of Angola and extend south-eastward across southern Africa into the southwest Indian Ocean[18,27,28]. Also extending south-eastward is the SICZ (blue dashed line **Box Fig. 1d**), which develops in southern summer and merges with the ITCZ over the southwest Indian Ocean[20]. The mid-level Botswana High, which forms in SON in response to heat released by rainfall over the Congo Basin, shifts southward and strengthens into its peak in DJF[29].

During March, April and May (MAM), the ITCZ moves into the equatorial and southern equatorial Africa region. Onshore moisture transport from the Indian Ocean leads to high rainfall, a period referred to as the "long rain" season[1,32] (**Box Fig. 1c**). Toward boreal summer, the ITCZ and the subtropical high-pressure systems move back at their northern-most positions.

Figures and Captions

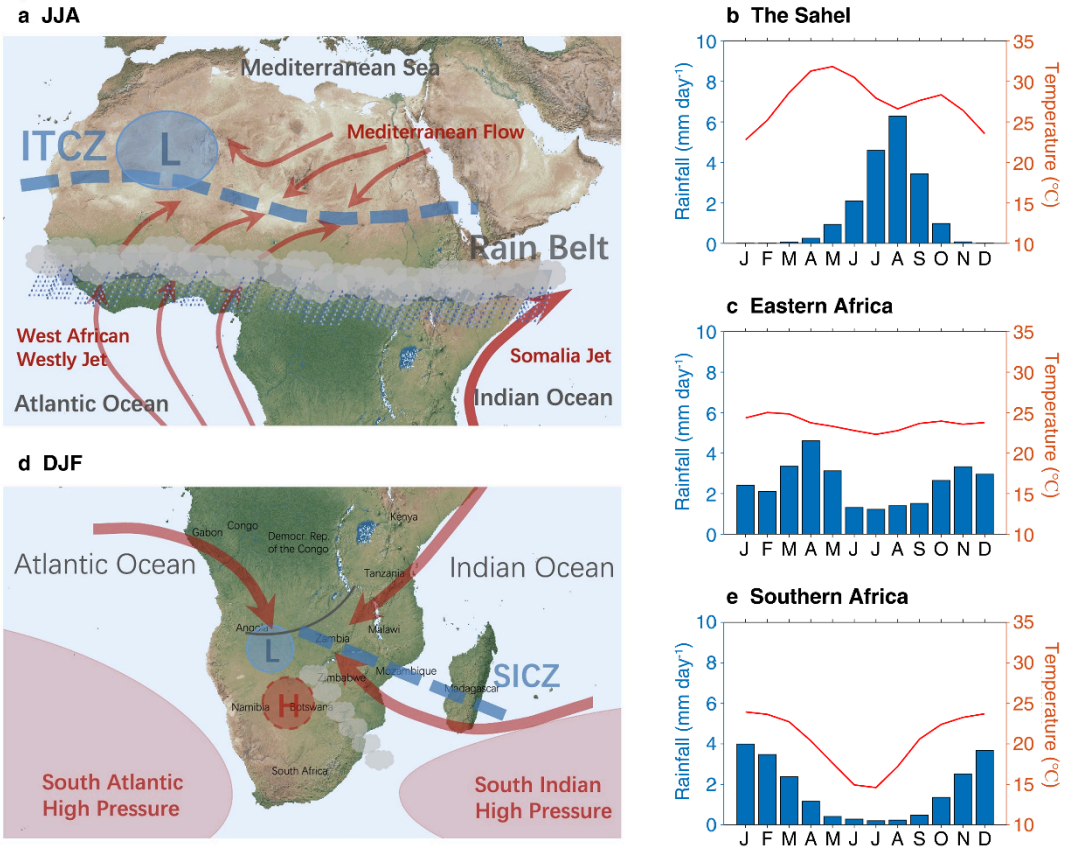

Box Fig. 1 | Climatological atmospheric circulation of Africa. **a**, Features related to Sahel summer rainfall, including low-level flows such as West African Westerly Jet and northerly winds of Mediterranean origin (thin red curved arrows) and Somali Jet (**thick** red curved arrow), the Saharan Heat Low (**blue L**), the Intertropical Convergence Zone (ITCZ, blue thick broken curve), and tropical rain belt (cloud and rain drops) Adapted from ref.[8]. **b-c,** Observed[169,170] seasonal rainfall and surface temperatures over the Sahel (17°W-40°E,11°N-15°N) and East Africa (29°E-42°E,7°S-5°N), respectively. **d,** Features associated with southern African summer rainfall, including the South Atlantic and South Indian high-pressure systems, the South Indian Convergence Zone (blue broken line, SICZ), and local circulation systems such as the Angola Low (blue L), Tropical Temperate Trough (cloud), and the Botswana High (dashed circle). Also shown is the Congo Air Boundary (black curved line) developing during September to November. Adapted from Refs[24,69]. **e,** Observed[169,170] seasonal rainfall and surface temperatures over Southern Africa (land over 24°E-42°E, 28°S-18°S).

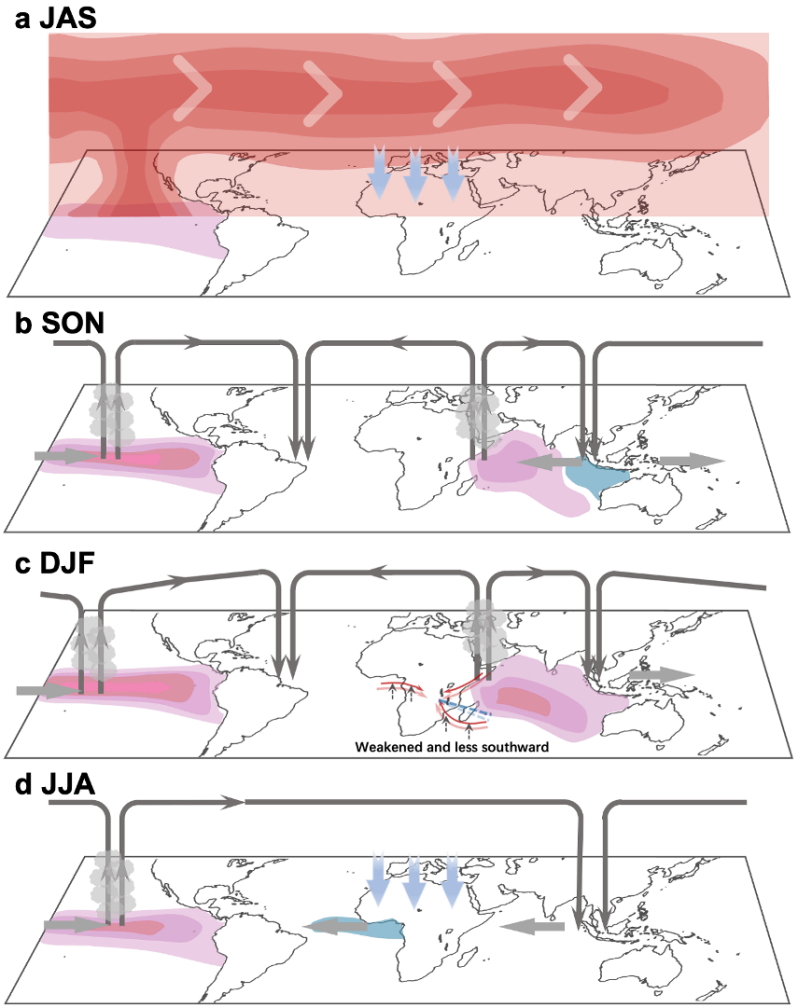

Figure 1 | Mechanisms of ENSO impact on African climate. a, Tropospheric temperature mechanism. During El Niño, anomalous ascending motion in the central and eastern equatorial Pacific triggers a Gill-Matsuno response and the associated atmospheric Kelvin waves distribute the tropospheric heating throughout the tropics (eastward arrows), increasing the atmospheric stability outside the Pacific, which suppresses (light blue downward arrows) atmospheric convection over West Africa[8], leading to decreased rainfall in the Sahel. **b, c,** Impact via the Indian Ocean. During El Niño, Walker circulation weakens leading to the development of positive IOD inducing anomalous rainfall in east Africa in the short rain season (**b**), and development of IOB warming reducing land-ocean pressure gradient such that the seasonal flow convergences and poleward excursion of the regional circulations weaken (**c**, indicated by contrast of climatological mean (light) and that during El Niño), and the SICZ shifts northeastward contributing to a rainfall dipole (northeast wet but southern dry). **d**, Impact via the Atlantic Ocean. During El Niño, Atlantic Niña, which shifts tropical rain belt northward, decreasing rainfall over the Guinea coast, with a tendency to increase rainfall over the Sahel. When an Atlantic Niña is dominated by an El Niño, reduced rainfall from the tropospheric temperature mechanism dominates (light blue downward arrows), generating dry anomalies over the Sahel.

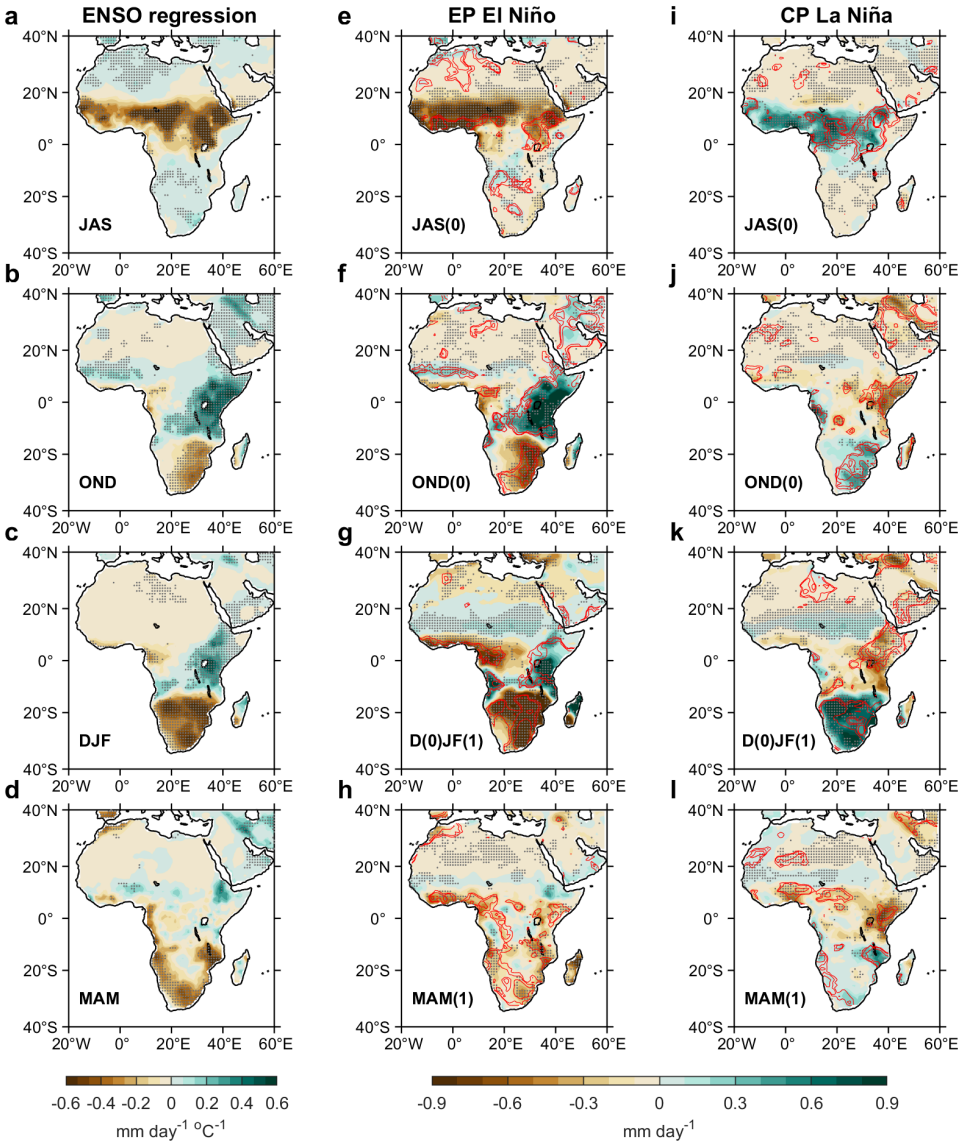

Fig. 2 | Seasonal evolution of El Niño impact on African rainfall. a, Observed July-August-September (JAS) anomaly pattern obtained by regressing anomalies from data/reanalysis[169,170,171,172] since 1948 onto a normalized concurrent Niño3.4 index[173,174,175]. Areas with statistical significance above the 95% confidence level is indicated by stipples. **b-c,** The same as **a** but for October-November-December (OND); **c,** December-January-February (DJF); and **d,** March-April-May (MAM) seasons, respectively. **c-h,** Composites of rainfall[169,170,171,172] (shading) anomalies for EP El Niño. during JAS, OND, DJF; and MAM. Red contours represent the 90%, 95% and 99% confidence levels. Stippled areas indicate that more than 70% of ENSO events have the same-signed anomalies. **i-l,** The same as **c-h** but for CP La Niña. ENSO affects different regions in different seasons through different mechanisms, for example, by forcing modes of SST variability in the Indian Ocean. The generally opposite impact between El Niño and La Niña is mostly due to that between EP El Niño and CP La Niña.

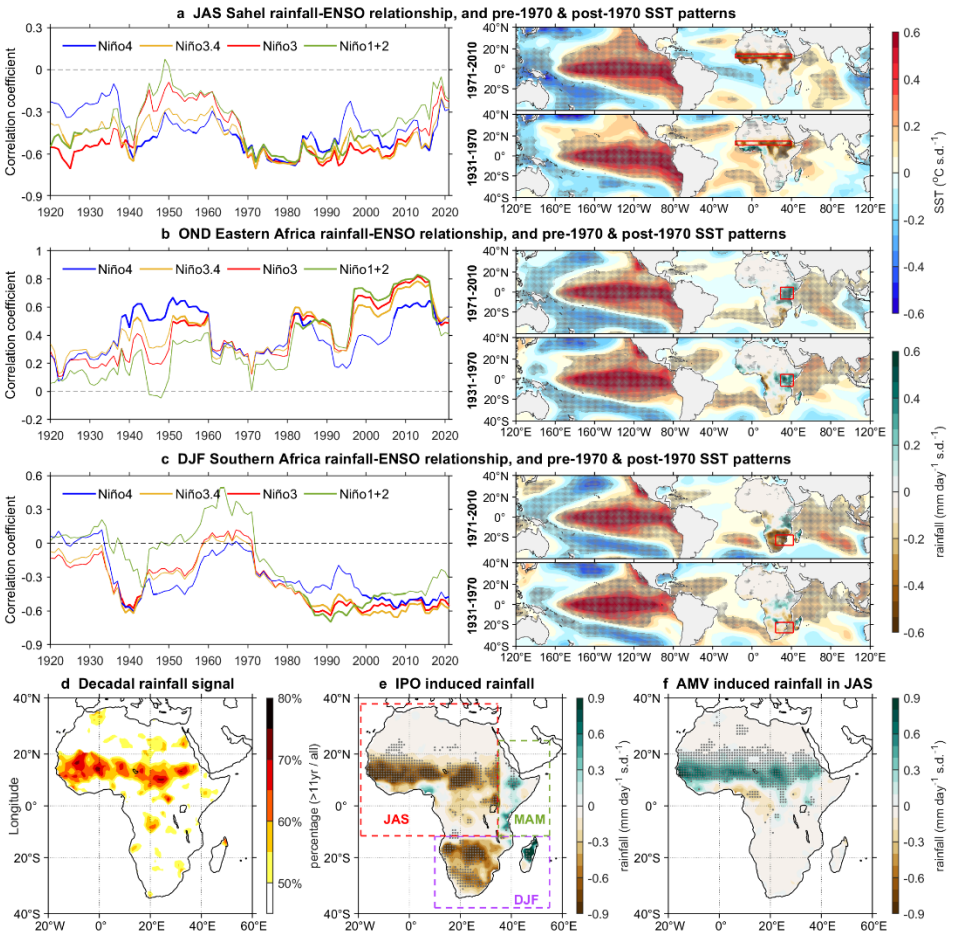

Fig. 3 | Influence from decadal variability. a, (Left) Observed 20-year moving correlation between Sahel rainfall anomalies (17°W-40°E,11°N-15°N; red box in the right panels) and different ENSO indices in July-August-September (JAS). Both rainfall anomalies and Niño indices are 11-year high-pass filtered before calculating the 20-year moving correlation. Thickened lines indicate statistical significance above the 95% confidence level. Years on the x-axis denote the end year of the 20-year sliding window. (Right) Regression of global SST (°C) and African rainfall (mm day^{-1}) anomalies onto normalized Niño3.4 index in 1971-2010 (upper) and in 1931-1970 (lower), respectively. Stippled areas indicate statistical significance above the 95% confidence level. **b-c,** As in **a,** but for October-November-December (OND) land rainfall anomalies over Eastern Africa (29°E-42°E,7°S-5°N), and for December-January-February (DJF) land rainfall anomalies over Southern Africa (15°E-40°E,35°S-15°S). **d,** Ratio of decadal rainfall variability (>11 year; s.d.) relative to total year-to-year rainfall variability in 1901-2022. **e,** Regression of seasonal rainfall anomalies (mm day^{-1}) in different parts of Africa onto a normalized 11-year low-pass filtered annual mean IPO time series[176]. We focus on JAS season in the western and northern Africa (20°W-35°E,12°S-40°N), March-April-May (MAM) season in the eastern Africa (35°E-55°E,12°S-25°N), and DJF season in the southern Africa (10°E-55°E,38°S-12°S). **f,** Regression of JAS rainfall anomalies (mm day^{-1}) onto normalized 11-year low-pass filtered annual mean AMV time series[177]. The SST and rainfall data are from ERSSTv5[178], and CRU TS v4.07[169], respectively, in

1901-2022. Decadal variability not only modulates ENSO impact but also induces decadal anomalies on which ENSO anomalies superimpose.

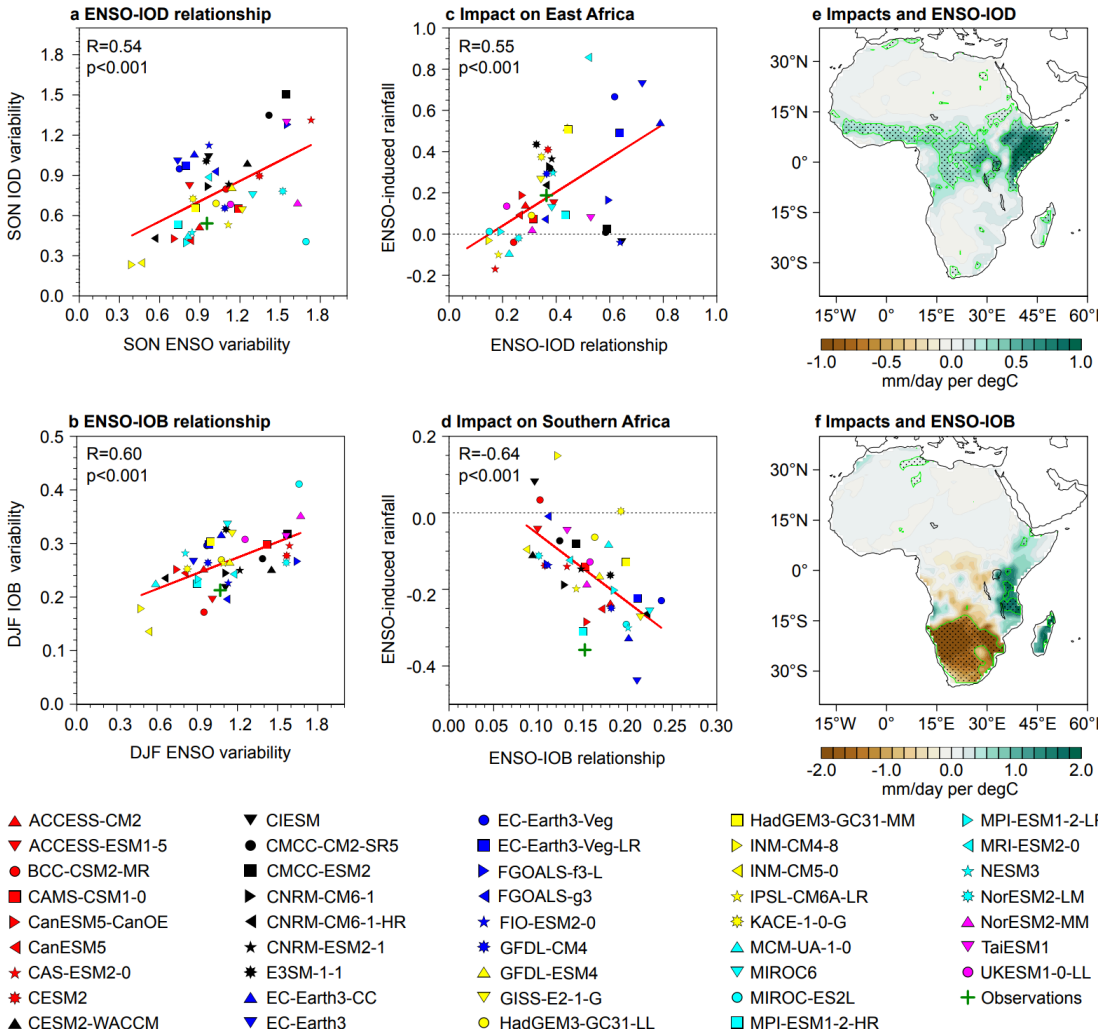

Fig. 4 | Simulated present-day ENSO influence on African rainfall via the IOD and the IOB based on CMIP6. a, Inter-model spread of simulated amplitude of ENSO and IOD variability in September-October-November (SON) (ºC). Linear fit is displayed together with correlation coefficient R and p value. **b,** Inter-model spread of simulated amplitude of ENSO and IOB variability in December-January-February (DJF) (ºC). **c**, Inter-model relationship between response of SON eastern Africa rainfall (Eq.-10°N, 35°E-45°E) to ENSO (mm day^{-1} ºC^{-1}) and response of the SON IOD index (ºC) to ENSO (ºC). The respone is defined as the linear regression coefficient. **d**, As in **c**, but for response of DJF southern Africa rainfall (15°S-40°S, 10°E-40°E) to ENSO and response of the IOB to ENSO. **e,** Inter-model relationship between response of grid-point SON rainfall anomalies (mm day^{-1} ºC^{-1}) to ENSO and response of the SON IOD index (ºC) to ENSO. **f**, The same as **e**, but for DJF rainfall and DJF IOB. Green and **brown** areas in **a** and **c** represent enhanced and **reduced** rainfall from ENSO, respectively. Stippling represents statistical significance at the 95% confidence level. The IOD index is defined as difference in SST anomalies over

the western tropical Indian Ocean (10°S-10°N, 50°E-70°E) and the eastern Indian Ocean (10°S-Eq., 90°E-110°E), and the IOB is defined as SST anomalies averaged over the tropical Indian Ocean (30°S-25°N, 40°E-110°E). Models in which the IOD and the IOB are more responsive to ENSO produce stronger rainfall anomalies during ENSO events.

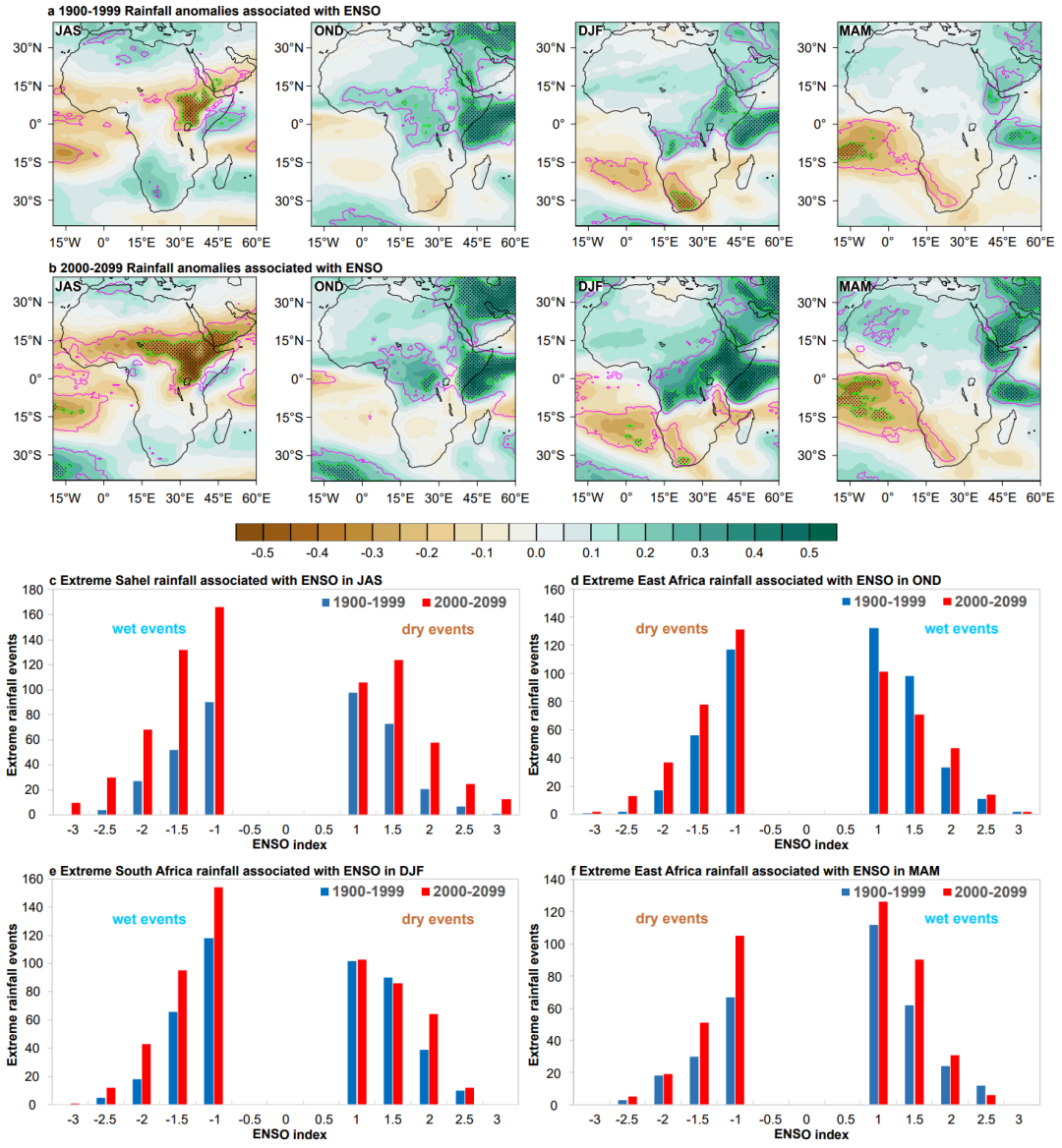

Fig. 5 | Future change of African rainfall associated with ENSO. Shown are aggregated over all models. **a, b,** Multimodel ensemble mean of regression of rainfall onto Niño3.4 for the 20th and 21st century, respectively, from left to right, in July-August-September (JAS), October-November-December (OND), December-January-February (DJF), and March-April-May (MAM); for each model, seasonal rainfall anomalies and Niño3.4 are quadratically detrended and normalized over the 1900-2099 period, and then separated into two 100-year periods. Areas confined by purple and green (with stippling) contours indicate where more than 50% and 70% of models agree on a 95% statistically significant correlation, respectively. **c**,

JAS dry (rainfall anomalies < -1.0 s.d.) and wet seasons (rainfall anomalies > 1.0 s.d.) over Sahel as a function of concurrent ENSO amplitude in 1900-1999 and 2000-2099 within a 0.5 bin. Left part shows the wet season number associated with La Niña (Niño 3.4 < -1.0 s.d.), right part shows the dry seasons associated with El Niño (Niño 3.4 > 1.0 s.d.). **d-f**, Same as **c**, but for OND east Africa rainfall, DJF south Africa rainfall, and MAM east Africa rainfall, respectively. In general, increased ENSO variability leads to a higher frequency of dry and wet extreme anomalies.

Acknowledgments

We are grateful to Prof. Jianping Gan of Centre for Ocean Research, Hong Kong University of Science and Technology, for hosting our workshop on "Climate Variability and Impact on Africa." Special thanks to his team for ensuring our Hong Kong workshop was productive scientifically, delightful culinarily and rewarding culturally, and to the Centre for providing vital support for hotels, meals, and venue, without which, this paper would not be possible. This project is supported by National Key R&D Program of China (2018YFA0605700). E.M. and B.R. received funding form the Spanish Ministry of Science and Innovation projects (PID2021-125806NB-I00 and TED2021-130106B-I00). G.W., B.N., A.S.T. and A.S. are supported by the Earth System and Climate Change Hub of the Australian Government's National Environment Science Program. S.L. was supported by the National Natural Science Foundation of China (NSFC) projects 42376198 and 42006173. PMEL contribution no. 5586. We acknowledge the World Climate Research Programme's Working Group on Coupled Modelling, which is responsible for CMIP, and we thank the climate modeling groups for producing and making available their model output, the U.S. Department of Energy's Program for Climate Model Diagnosis and Intercomparison for coordinating support and leading development of software infrastructure in partnership with the Global Organization for Earth System Science Portals. We are grateful to various reanalysis groups for making the datasets available to us.

Author contributions

W.C. and M.J.M conceived the study. The manuscript was written as a group effort through participation in several "Climate Impact on Africa" workshops held online and at Hong Kong University of Science and Technology. W.C designed the study and coordinated the writing. A.S. synthesized workshop key points. J. M. led C.R., and E.M., B.R. led discussion and revision of section 2, 3, and 4. X. L., B.N., Y.L., and T. G. conducted data analysis and created the Figures. All authors contributed to the manuscript preparation, interpretations, and the discussions.

Competing interests

The authors declare no competing interests.

Data and materials availability

All observation and model datasets used here are publicly available or available on request.